## PALACKÝ UNIVERSITY OLOMOUC

#### **FACULTY OF SCIENCE**

#### DEPARTMENT OF PHYSICAL CHEMISTRY



### **Modeling of Biomembranes**

#### Annotation of Doctoral Thesis

Author: Mgr. Martin Šrejber

Supervisor: doc. RNDr. Karel Berka, Ph.D.

Consultant: prof. RNDr. Michal Otyepka, Ph.D.

Study programme: Chemistry

Study field: Physical chemistry

Study form: Daily

Olomouc 2023

Jméno a příjmení uchazeče: Mgr. Martin Šrejber

Typ práce: Disertační

Pracoviště: Katedra fyzikální chemie

Studijní program: Chemie

Studijní obor: Fyzikální chemie

Vedoucí práce:doc. RNDr. Karel Berka, Ph.D.Konzultant:prof. RNDr. Michal Otyepka, Ph.D.

Oponenti: doc. RNDr. Radka Svobodová, Ph.D.

Central European Institute of Technology & National Centre for Biomolecular Research,

Faculty of Science Masaryk University

Kamenice 5, Bohunice, 625 00 Brno

Assoc. Prof. Gabin Fabre, Ph.D.

INSERM U1248

Pharmacology and transplantation

University of Limoges

France

#### **List of Publications:**

- 1. **Šrejber M.**, Navrátilová V., Paloncýová M., Bazgier V., Berka K., Anzenbacher P., Otyepka M. Membrane-attached mammalian cytochromes P450: An overview of the membrane's effects on structure, drug binding, and interactions with redox partners. (2018) *J. Inorg. Biochem.* 183. 117-136. (https://doi.org/10.1016/j.jinorgbio.2018.03.002)
- IF in 2018: 3.224
- 2. Juračka J.<sup>†</sup>, **Šrejber M.**<sup>†</sup>, Melíková M., Bazgier V., Berka K. MolMeDB: Molecules on Membranes Database. (2019) *Database*. 2019. baz078 (https://doi.org/10.1093/database/baz078) IF in 2019: 2.331

- 3. Balouch M., **Šrejber M.**, Šoltys M., Jánská P., Štěpánek F., Berka K. In silico screening of drug candidates for thermoresponsive liposome formulations. (2021) *Mol. Syst. Des. Eng. 6.* 368-380 (https://doi.org/10.1039/D0ME00160K)
- IF in 2021: 3.323

#### List of other publications not involved in this thesis:

Paloncýová M., **Šrejber M.**, Čechová P., Kührová P., Zaoral F., Otyepka M. Atomistic Insights into Organization of RNA-Loaded Lipid Nanoparticles. (2023) *J. Phys. Chem. B.* 127 (5) 1158-1166

Paloncýová M., Čechová P., **Šrejber M.**, Kührová P., Otyepka M. Role of Ionizable Lipids in SARS-CoV-2 Vaccines As Revealed by Molecular Dynamics Simulations: From Membrane Structure to Interaction with mRNA Fragments. (2021) *J. Phys. Chem. Lett.* 12 (45) 11199-11205

Pykal M., Vondrák M., **Šrejber M**., Tantis I., Mahammadi E., Bakandritsos A., Medved' M., Otyepka M. Accessibility of grafted functional groups limits reactivity of covalent graphene derivatives. (2022) *Appl. Surf. Sci.* 598. 153792

Annadurai N., Malina L., Salmona M., Diomede L., Bastone A., Cagnotto A., Romeo M., **Šrejber M.**, Berka K., Otyepka M., Hajdúch M., Das W. Antitumour drugs targeting tau R3 VQIVYK and Cys322 prevent seeding of endogenous tau aggregates by exogenous seeds. (2021) FEBS J. 289. 1929-1949

<sup>&</sup>lt;sup>†</sup>Authors contributed equally.

## Outline

Outline	- 4 -
1. Motivation	- 6 -
2. Biomembranes	- 7 -
2.1 Lipids as building blocks	- 7 -
2.2 Membrane structure and physical properties	- 10 -
3. Interactions of drugs with membranes	- 12 -
3.1 Effect of membrane composition	- 14 -
3.2 Calculations of Drug Permeabilities	- 15 -
4. Membrane proteins	- 19 -
4.1 Cytochrome P450 enzymes	- 19 -
4.2 Cytochrome P450 reductase	- 22 -
5. Results	- 24 -
5.1 MolMeDB project	- 25 -
5.1.1. MolMeDB user interface	- 27 -
5.1.2. Case study	- 28 -
5.2 Permeation of cyclosporin A through biomembranes	- 30 -
5.2.1 Cyclosporin A behavior on membrane models	- 33 -
5.2.2 Conclusions on cyclosporin A	- 34 -
5.3 In silico screening of drug candidates for temperature-responsive	liposome
formulation	- 35 -
5.3.1. MD simulation of bilayer phase transition	- 36 -
5.3.2. COSMO-based partitioning and permeability calculations fort fluorescent dyes	- 36 -
5.3.3. Selection criteria encapsulation/thermoresponsive release and DrugBank screening	- 37 -
5.4 Behavior of Mitochondrial Cytochrome P450 11A1 on DOPC and Mitochond	chondrial
Membrane Models	- 40 -
5.4.1 Behavior of CYP11A1 on DOPC	- 41 -
5.4.2. Interaction of CYP11A1 with mitochondrial membrane	- 43 -
5.4.3. CYP11A1 channels dynamics	- 47 -
5.4.4. Interaction of CYP11A1 with Adrenodoxin	- 48 -
	A

5.5 Membrane-attached Model of Cytochrome P450 Reductase: Simulations of natural		
occurring states and of the complex by cytochrome P450 3A4	- 49 -	
5.5.1 Models of CPR in closed and open conformations	- 49 -	
5.5.2 Model of membrane-attached CPR-CYP 3A4 complex	- 52 -	
6. Summary	- 54 -	
7. References	- 56 -	

#### 1. Motivation

Computational chemistry is dynamically developing field of chemistry allowing us to understand the atomistic nature underlying all variety of naturally occurring phenomena. Especially nowadays with the exponential increase of computational power resources it allows us to tackle myriad of issues yet unreachable until today. The scope of computational chemistry ranges from studies related to solving of electronic states of systems by means of quantum mechanics (QM) usually limited by the size of studied systems up to dynamical studies by means of molecular dynamics simulations (MD) that are directly matching the sizes (nanometers) and time scales (microseconds) of experimental techniques. Molecular dynamics plays especially significant role in *in silico* study of biological processes and rationalizing the atomistic principles originating from them.

This thesis is focused on employment of theoretical tools (MD simulations, enhances sampling techniques, database data utilization) in study interactions of biological membranes with another naturally occurring species. The theoretical part of this thesis is focused on biomembranes itself i. e. their composition diversity, function and how they interact with drugs. It also briefly describes some essential proteins (cytochromes P450s (CYPs) and its redox partner cytochrome P450 reductase (CPR)) for which the interaction with biological membrane is vital and that are later discussed in result sections. The methodology section is focused on theoretical approaches and strategies used to study either biomembranes itself or their interaction with another chemical species. Finally, the Results chapter summarizes:

- the development and usage of MolMeDB database. This database was design to systematically collect, validate and visualize data related to molecule-membrane interaction
- ii. the permeation of widely used immunosuppressant cyclosporin A through several biological membrane models
- iii. the development and validation of systematic computational methodology for prediction of suitable liposomal encapsulation and thermally induced release of bio-active compounds
- iv. the effect of membrane composition on behavior of microsomal cytochrome P450 CYP11A1
- v. the behavior of membrane-attached cytochrome P450 reductase and its interactions of its redox partner cytochrome P450 CYP3A4.

#### 2. Biomembranes

Biological membranes allow life as we know it. They are essential components of all biological cells, living systems and organisms. Biomembranes' key role originates from their structure, complexity of composition, physical-chemical properties, and irreplaceability in multiple biological processes. We define them as two-dimensional liquid composed of lipids and protein arrange primarily into the form of a lipid bilayer. This highly dynamical complex functions as a natural barrier between subcellular compartments and cell segregation from the external environment. In skin cells, membranes protect the human body from the intrusion of noxious substances. Due to their selective permeability, they control the flux of substances going through them. Biomembranes also serve as a matrix to anchor proteins involved in a variety of biological processes. They mediate the communication between individual compartments via protein capable of conformation changes or control chemical and electrical signals.

#### 2.1 Lipids as building blocks

Lipids are a diverse group of macromolecules soluble in nonpolar solvents and insoluble in polar solvents, such as water. Lipids themselves are generally composed of "building blocks" such as alcohols, phosphates, glycerol, sphingosines, and fatty acids that characterize final lipid molecules' unique properties. In mammalian cells, the most abundant lipids components are glycerophospholipids, sphingolipids and sterols.<sup>1</sup>

**Glycerophospholipids** (GPLs) are the main building blocks of biomembranes, including plasma or organelle membranes. These constitute of sn-glycerol-3-phosphate backbone esterified by free fatty acids in positions sn-1 and sn-2. Subsequently, the phosphate is bound to a variety of alcohol groups. The chemical diversity of GPLs is determined by the interplay between various fatty acids, sn-1 linkage to glycerol and the head group. The polar head groups consist of negatively charged phosphate moiety bound to alcohol substituent (Figure 1).

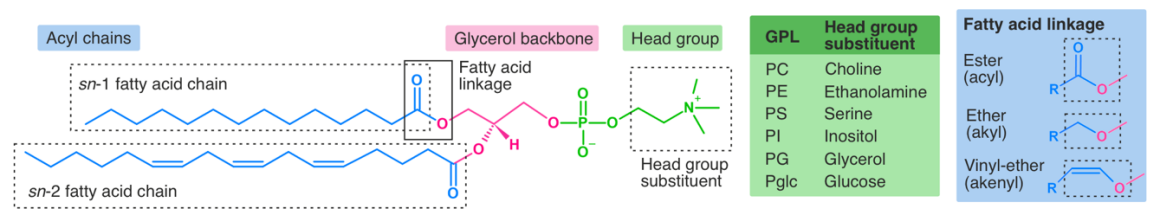


**Figure 1.** The structural diversity of glycerophospholipids. The structural diversity of individual lipids originates from a variety of acyl chains (blue), glycerol linkage (pink) and the choice of head group substituents (green).

The alcohols are bound to the phosphoryl group via -OH group and can be classified based on their charge as positively charged (choline, ethanolamine), neutral (glycerol, inositol) or neutral zwitterions (serine) (Figure 2). This interplay between negatively charged phosphates and variable charges of alcohol substituents determine the overall charge of lipids, e.g., phosphatidylcholines (PCs), phosphatidylethanolamines (PEs) and phosphatidylinositols (PIs) are neutral (zwitterionic) lipids due to the compensation of opposite charges. Similarly, phosphatidylserines (PSs) and phosphatidylglycerols (PGs) bear an overall negative charge. The chemical structure of alcohols affects their ability to intermolecular interactions through the hydrogen bonds network. Lipids with more polar alcohol substituent (ethanolamine, glycerol and serine) serve as proton donors and acceptors for hydrogen bonds, while more minor polar alcohol groups (choline) cannot form hydrogen bonds. Head group electrostatics, shape and the hydrogen bond acceptor/donor capacity significantly affect the interaction between individual lipids and molecules' permeation through membranes or membrane-protein interaction.

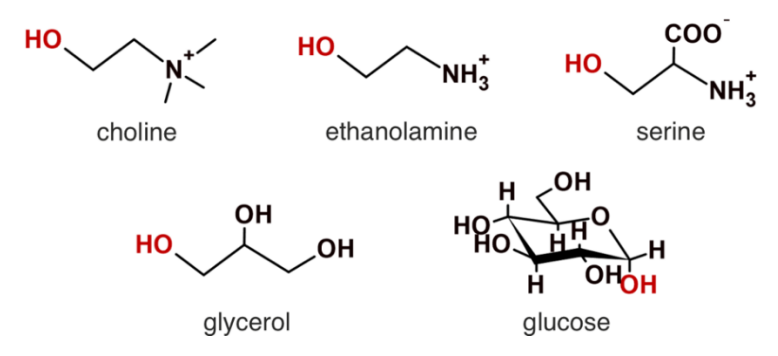


Figure 2. Example of head group substituents in glycerophospholipids.

Another aspect contributing to lipid structural diversity is the linkage between free fatty acids and the phosphoryl group. The linkage can be mediated either by ester, ether or vinyl-ethers (Figure 1). The vast majority of GPLs are acyl ester lipids. Alkyl ether (and alkenyl vinyl-ether) lipids, such as plasmalogens, constitute up to 20% of the total phospholipid mass in humans and are primarily localized in brain and heart tissue.<sup>3</sup>

The most important and structurally diverse constituents of lipids are fatty acids. Their variance originates from the variability of carbon chains length and the degree of saturation. The typical length of free fatty acids varies between 14 to 20 carbon atoms. More than half of naturally occurring fatty acids is unsaturated. The sn-2 fatty acid chain is usually mono- or polyunsaturated, whereas the sn-1 fatty acid chain is usually fully saturated. The first saturations generally occur at C3 ( $\omega$ -3) and C6 ( $\omega$ -6) carbon atoms (numbered from terminal methyl group). Most fatty acids have a double bond in cis configuration resulting in  $\sim$ 30° bend in the hydrocarbon chain, whereas the trans configuration leads to a straight hydrocarbon chain. The presence of cis double bond

configuration decreases the ordering of lipid tails hence increases the fluidity membrane.<sup>4</sup> The occurrence of triple bond and conjugated double bonds is rare.

Another important lipid component of biomembranes is **sterols**. In plants and yeasts, the most abundant type is ergosterol, whereas plants' membrane composition is more complex and contains a mixture of sterol, e.g., cholesterol, campesterol, stigmasterol or sitosterol. Cholesterol (CHOL) is the most abundant sterol in the mammal. Although the ratio of cholesterol varies in individual membranes. From a structural point of view, the cholesterol consists of semi-rigid fused rings with -OH group and aliphatic chain bound opposite sides of ring structure (Figure 3). Cholesterol plays a crucial role in maintaining membrane rigidity and ordering. The increasing amount of cholesterol in the liquid-disordered ( $L_d$ ) phase results in membrane transition into a stiffer and thicker liquid-ordered ( $L_o$ ) phase. It is hypothesized that cholesterol is also involved in the formation of  $L_d/L_o$  phase-separated microdomains, so-called lipid "rafts".

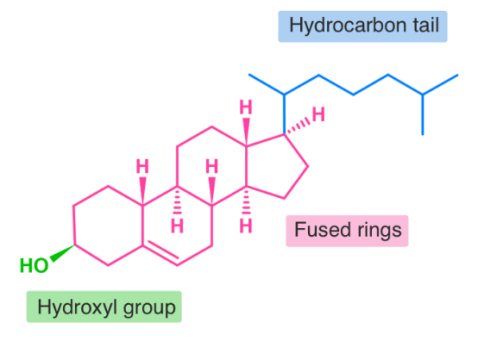


**Figure 3.** The structure of cholesterol.

Sphingolipids are composed of sphingoid base backbone, acyl chain and head group substituents (Figure 4). The sphingolipids' diversity arises from various lengths, degrees of saturation, and hydroxylation of the sphingoid base backbone. The N-acyl chains of sphingolipids are usually more saturated and longer when compared to acyl chains in GPLs. Similarly to GPLs, the head group substituents are diverse and vary in shape and charge. The small hydroxyl group's connection to the serine moiety will lay the structural foundation for ceramide lipids (CERs), whereas phosphocholine's linkage will form sphingomyelins (SMs). Furthermore, the addition of saccharide group form glycolipids, e.g., glycosphingolipids (sphingoid base backbone bound to one or multiple sugars via ether bond) or glycophosphatidylinositol (sphingoid base backbone bound to PI moiety).

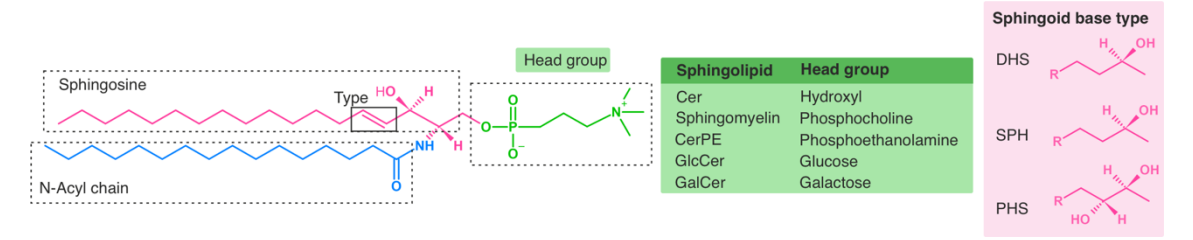


Figure 4. Structural bases of sphingolipids.

#### 2.2 Membrane structure and physical properties

The membrane is composed of lipid molecules separated into two distinguishable leaflets that act as a two-dimensional fluid. The formation of lipid bilayers originates from the amphipathic nature of lipid molecules, having the hydrophilic head region exposed to the aqueous environment and the hydrophobic tail region tightly packed core of the membrane. The amphipathic character causes the self-assembly of lipids in water into various shapes, starting from simple lipid bilayers into more complex vesicles and liposomes, depending on lipid structural parameters (head group substituent, length and saturation of acyl chains) and external factors such as temperature and pressure. The bilayer arrangement of membranes is driven to maximize the membrane surface and minimize the internal volume.

In eukaryotes, more than 50% of all GPLs found in membranes are phosphatidylcholines (PC). The head group's proportional size and the aliphatic tail make the overall molecular shape of PCs cylindrical. Structurally, they arrange into lamellar bilayers with no curvature strain. Lipids with proportionally smaller lipid head groups (PEs) and the asymmetrical truncated cone shape tend to form nonlamellar inverted hexagonal structures due to the negative curvature stress. The unsaturation of acyl chains further increases this behavior. In contrast, lipids with bulkier head groups (PIs, single acyl chain lipids, detergents) opposite to tail region and inverted conical lipid shape that induces positive curvature strain forms hexagonal structures.<sup>7</sup>

Apart from the membrane shape, lipid composition also strongly affects the lipid membrane phase. Membrane phase behavior originates from specific lipid-lipid interaction, and it is described by lipid parameters such as lipid order parameters ( $S_{CD}$ ) or lateral diffusion coefficient ( $D_L$ ) (Figure 5). At room temperature, most abundant mixtures of GPLs with longer and unsaturated carbohydrates are found in the  $L_d$  phase defined by low ordering acyl chains and high lipid mobility. Decrease of temperature or change of composition towards more saturated (sphingolipids) or longer acyls (e.g., stearic acid) lipids induce the phase transition into rigid solid gel ( $S_o$ ) phase. Tight packing of lipids causes higher ordering of lipids and slow lateral diffusion. The addition of sterol molecules into the lipid mixture (binary or tertiary) forms a liquid-ordered phase that is highly ordered but highly fluid.

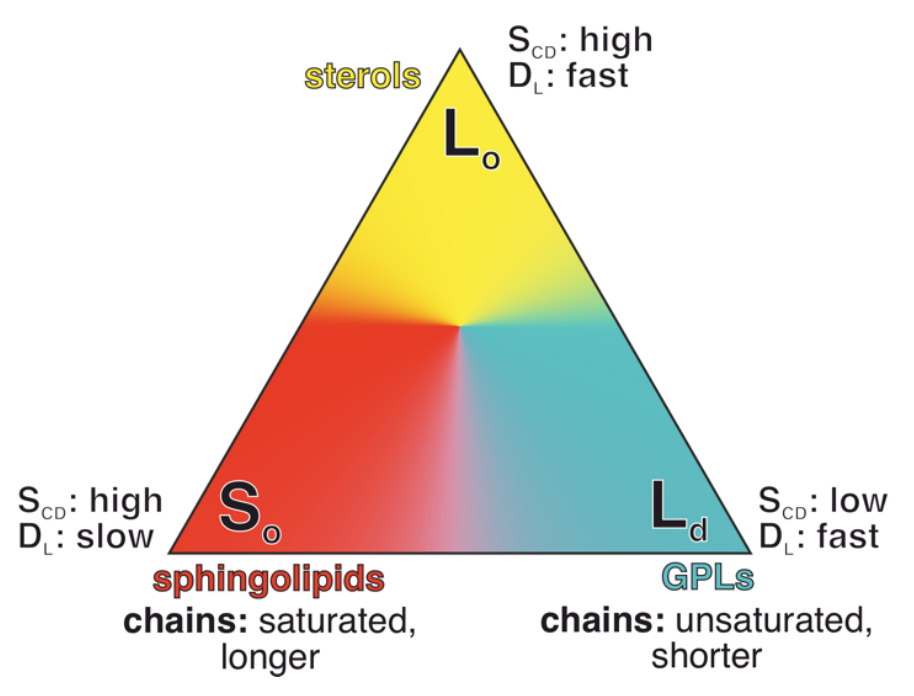


**Figure 5.** Lipid phase diagram. Cholesterol enriched membranes are found in the  $L_0$  phase defined by low order parameters and fast lipid diffusion. At a human body temperature, the  $L_d$  is the predominant membrane phase with the low ordering of acyl chains and fast lipid diffusion. The solid gel  $S_0$  phase is the preferential phase for sphingolipids.

It is not easy to describe all the membranes' physical properties only on account of lipid composition diversity. For this purpose, a set of fundamental parameters describing membrane structure and dynamics is defined. Both experimental and theoretical techniques can obtain those qualitative parameters, and the combination of those approaches helps to understand the structural nature of membranes.

#### 3. Interactions of drugs with membranes

The interaction of small molecules (drugs, xenobiotics, endobiotics, ligands, etc.) with membranes plays a crucial role in multiple physiological processes, and therefore a thorough understanding of the mechanism of drug-membrane interaction and consequential permeation is needed. The drug uptake (oral, intravenous, transdermal, intramuscular) passes through various biomembranes before reaching its target. Hence, the drug's ability to permeate those natural barriers may be the limiting step in drug absorption, distribution, metabolism and excretion (ADME).

The drug-membrane crossing can occur by many routes depending on the drug's chemical nature and external factors. Small and moderately polar and uncharged compounds can passively **diffuse across** the membrane without any energetical penalty. Here the process is driven simply by concentration gradients. This is especially noticeable for nonpolar small gasses like  $O_2$ ,  $N_2$ ,  $CO_2$ . In case of small polar solvents such as ethanol or water—the passive diffusion is slower (by approximately three orders of magnitude) yet present. <sup>8,9</sup> Also small but less polar (more hydrophobic) compounds like benzene can diffuse passively through membranes. It is worth mentioning that even some larger and more polar molecules like Cyclosporin A (CsA) – an orally active immunosuppressant – are known to permeate passively even though their permeability is relatively low compared to typical smaller permeants.

Molecules that are not permeable using simple diffusion can be transferred across the cell membrane either by **facilitated diffusion** or **active transport**. The first of the mentioned utilizes the drug transport by transmembrane protein pores. This includes, for example, the aquaporin protein channels family (AQP) or the glucose transporters family (GLUT) responsible for glucose uptake. The latter governs drug influx and efflux via transmembrane carriers against a substrate concentration gradient. Active transport usually requires significant conformational changes of protein structure and energy use in the form of adenosine triphosphate (ATP). Here belongs the ATP-binding cassette (ABC) transporters or the solute carrier (SLC) transporters' family.

The last route of transmembrane transport is **endocytosis**. In this process, part of the plasma membrane surrounds and "devours" the permeant. The pocket with its cargo consequently detaches and is transported in the form of vesicles. In this way, even large macromolecular objects like viruses or whole bacteria can be transferred to cells.<sup>10</sup>

In assessing the permeability, Lipinski's rule of five<sup>11</sup> criteria generally defines the basic set of physicochemical descriptors for orally active compounds. It predicts that the molecule is potent after oral administration when:

- *i.* the molecular weight is below 500 Da,
- ii. there are less than five hydrogen bond donors,
- iii. there are less than ten hydrogen bond acceptors,
- *iv.* an octanol/water partition coefficient ( $log K_{o/w}$ ) is lower than 5.

Those simple descriptors can be extended by other parameters to improve permeability predictions of small molecules. Alike molecular weight, the increase of molecular volume decreases the permeability of the permeant. The polarity of the molecule, another key property in assessing the molecule permeability, can be implemented by adding a polar surface area (PSA) descriptor. Generally, the increase of molecular polarity decreases the ability to permeate passively. The capability of compounds (usually cyclic peptides) to form intramolecular hydrogen bonds also increases their permeability. Usually, a combination of multiple descriptors is used to achieve a better permeability prediction score, e.g. Potts and Guy model for skin permeability based on molecular weight/volume and  $\log K_{o/w}$  15

$$\log K_P = \log \left(\frac{D^0}{\delta}\right) + f \times \log K_{o/w} - \beta'' \times MW \tag{1}$$

where  $D^0$  is the diffusivity of a hypothetical molecule with zero volume, f coefficient accounts for the difference between the partitioning domain presented by octanol and that presented by the stratum corneum lipids, MW stands for molecular weight,  $\beta''$  is constant (0.0061) and  $\delta$  is diffusion path length.

The description of drug-membrane interaction is focused mainly on drug partitioning, permeability, diffusion, and its position in the membrane. **Partitioning** depicts the number of molecules dissolved in membrane and is described by lipid(membrane)/water partition coefficient  $\log K_{m/w}$ :

$$K_{m/w} = \frac{c_{lipid}}{c_{water}} \tag{2}$$

where  $c_{lipid}$  and  $c_{water}$  are concentrations of drug in lipid and water environment, respectively. The partition coefficient defines the ratio of concentrations of molecule distributed between lipid and water phases. Partitioning is sometimes used to describe the lipophilicity (i.e., affinity toward the lipid phase) of molecules.

In passive permeation, the drug is subjected to resistance from the membrane while being transferred. This solute resistance is proportional to the concentration of the drug being transferred and is therefore indirectly related to the solute's permeability. The **permeability** is defined in Fick's first law of diffusion as the steady-state flux of solute across the membrane and can be calculated as follows:

$$P = \frac{1}{R} = \frac{J}{\Lambda c} \tag{3}$$

where R is resistance, J is the flux of the solute, and  $\Delta c$  is its concentration gradient.

Membrane permeation can be described by a simple model (homogeneous solubility-diffusion model) in which the solute permeates between two aqueous compartments separated by a homogeneous oil slab (mimicking the membrane). Thus, the permeability coefficient is directly connected to the membrane thickness and **diffusion of the solute** by the following equation:

$$P = \frac{K_{m/w}D}{h} \tag{4}$$

where D is the diffusion coefficient of solvent and h is the thickness of the oil phase. It also shows how permeability is directly connected to the lipophilicity of the molecule. The less lipophilic molecule will permeate slowly than more lipophilic ones for two molecules with the same diffusion coefficient with similar size.

#### 3.1 Effect of membrane composition

The aforementioned varieties in biomembrane compositions cause differences in the physical properties of membranes. Those also affect the nature of interactions of the drug with biomembranes.

One of the key structural features that define membranes' properties – and consequently the drugmembrane interactions – is their lipid head group constituent. The effect of the head group region is rationalized mostly by theoretical studies. Permeation study of curcumin (therapeutic agent in cancer treatment) shows a higher affinity towards negatively charged DOPG lipid bilayer than DOPC membrane due to DOPG capacity to form hydrogen bonds. Another theoretical prediction of water permeation showed that the translocation process is driven by the membrane phase (liquid disordered and solid gel phases studied) rather than by the lipid head group composition. The permeation study of cytochrome P450 (CYPs) substrates/metabolites revealed slightly preferential partitioning into DOPC than into POPG membrane. Comparative study on single-component lipid membrane permeability by Mathai et al. concluded that permeability is related strongly to the area occupied by lipid rather than bilayer thickness.

As state above, cholesterol, as a major lipid component in many membranes, plays a crucial role in maintaining membrane phase and rigidity. The increase of cholesterol content in phospholipid membranes decreases the molecular motion of lipid tails and increases molecular packing, consequently observed as an increase in membrane ordering. Cholesterol was shown to reduce water permeability, and this decrease is proportional to its concentration in the membrane. Furthermore, it reduces the permeability of both cations (Na<sup>+</sup>, K<sup>+</sup>) and anions (Cl<sup>-</sup>) as well as sugars (glucose) through various prototypical membranes (PCs, PSs, PGs). PGs). In general, this shows that the decrease of permeability after the addition of cholesterol is independent of the surface charge of membranes. Cholesterol also reduces the permeability of quinine-based photodynamic drugs (hypericin and its derivates) in mixtures with DPPC. The reduction of permeability was different for individual derivates and cholesterol content (9 and 25 mol%). The partitioning of small drugs (ammonia, ethanol, nitric oxide, benzene, propane and neopentane) into the lipid tails region also decreases with cholesterol. The effect of cholesterol-induced decrease of permeability is more profound in the presence of saturated lipids and membranes with smaller lipid head groups (PE as compared to PC).

#### 3.2 Calculations of Drug Permeabilities

The first step in prediction of drug-membrane permeabilities is the calculation of free energy profile with respect to the membrane normal (described above). Generally, the free energy profile can denote the energetical information of membrane crossing event along defined pathway (Figure 6). It defines the height of the penetration barriers ( $\Delta G_{PEN}$ ) which are the time-limiting steps of crossing events. The affinity of drugs towards the membrane is also captured as the height of the membrane/water barrier,  $\Delta G_{WAT}$ , which usually correlates well with the partitioning coefficient logK<sub>m</sub>. It also determines the depths of the permeation as the position of the free energy minima ( $Z_{MIN}$ ).

Once the permeability calculations are performed and the free energy across given path is enumerated the task is to predict properties characterizing the membrane permeability itself e.g., the **permeability** and **diffusion coefficients** and drug **partitioning into membrane**.

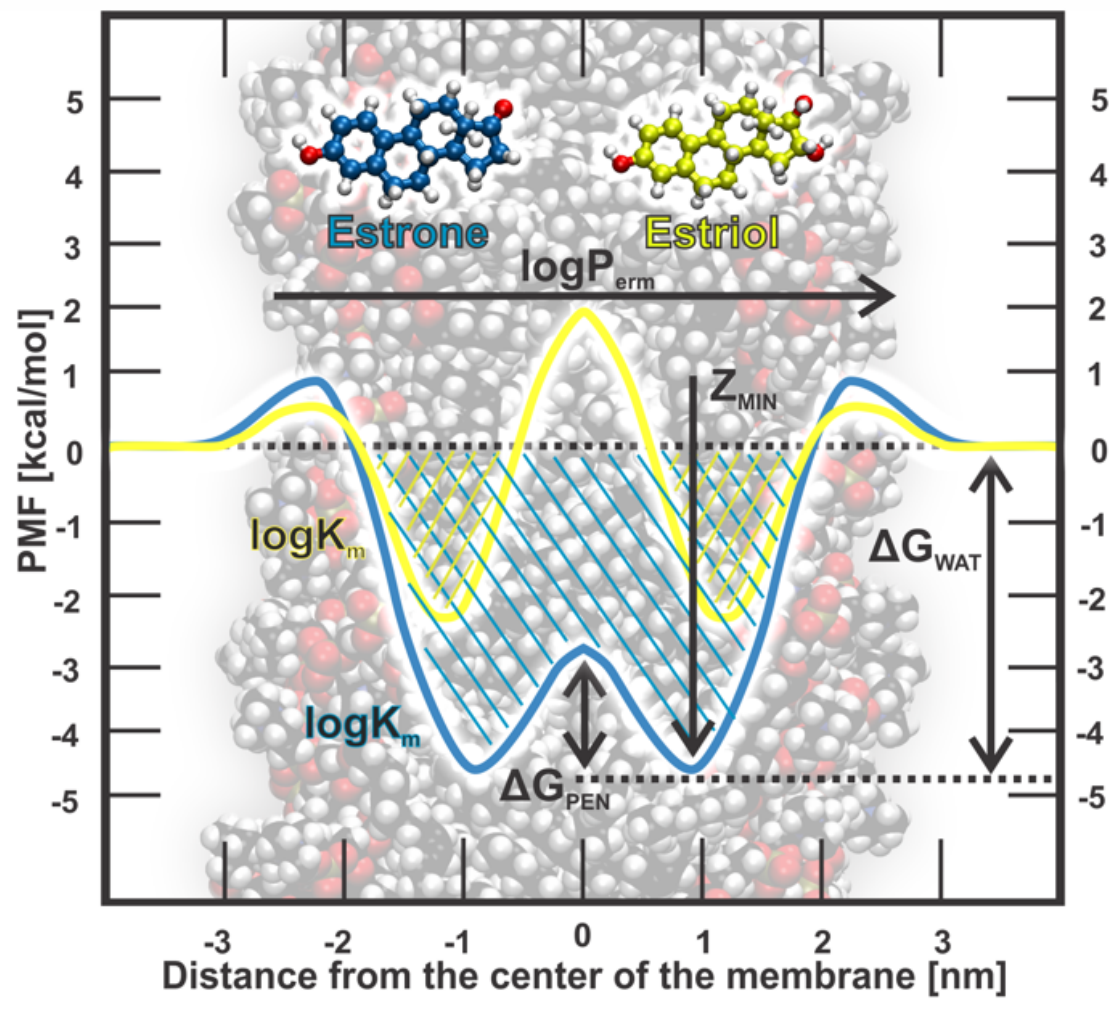


**Figure 6.** Overall schematic representation of the permeation process on example of two steroid molecules. The height of the penetration barriers ( $\Delta G_{PEN}$ ) and the affinity towards the membrane ( $\Delta G_{WAT}$ ) are calculated directly from the corresponding the energetical profile. The  $Z_{MIN}$  defines energetically preferential position along followed pathway.

Early concepts of cell permeabilities were proposed by Overton, simplifying the membrane permeability as transport through homogeneous oil slab where permeability coefficients correlate with oil/water partition coefficients. Here the permeation process depends only on the thickness of bulk solvent (oil) and the ability of solute to passively diffuse. In contrary to isotropic hydrophobic oil medium, membranes are highly heterogeneous and anisotropic systems. Their heterogeneity arises from its varying lipid composition and can be characterized by density distributions, order parameters or lipid diffusion. Besides, lipids consist of highly polar moieties, like glycerol/ester containing head groups, that could not be represented by simple oil phase. Overton's model was therefore not sufficient in depicting the structural and dynamic properties of membranes as transport medium.

More sophisticated model, so called *inhomogeneous solubility-diffusion model* was proposed encompassing the membrane heterogeneity. Here properties underlying the transport phenomenon depend on the depth of permeation and vary locally during molecule translocation. The overall **permeability coefficient** is than calculated as if the membrane was divided into finite number of layers in an integral form

$$P = \frac{1}{R} = 1 / \int_{z_1}^{z_2} R(z) dz = 1 / \int_{z_1}^{z_2} \frac{exp\left(\frac{\Delta G(z)}{k_B T}\right)}{D(z)} dz$$
 (5)

where R(z), D(z) and  $\Delta G(z)$  are solute resistance, diffusion coefficient and free energy of transfer, respectively, at given position z along the membrane normal. Due to the exponential character of  $\Delta G(z)$  in the denominator, more appreciable changes of the permeability coefficient are found for systems with positive free energy values, while the partitioning into the membrane is neglected.

The overall **partitioning coefficient** in the membrane/water environment, integrated over membrane and water regions, can be calculated from free energy profile as

$$K = \int_{z_1}^{z_2} exp \left( \frac{-\Delta G(z)}{k_B T} \right) dz \tag{6}$$

Since the partitioning defines the ration of concentrations of molecules between the membrane and the water phase it is necessary to define the boundaries between those two phases. Defining the exact borders is not trivial task, since biological membranes are predominantly found in disordered phase which is highly flexible and with inclinations to undulations. An elegant way around it was proposed by Klamt et al., by weighting the free energy based on the ratio of density of water in each layer  $\rho_{(z)}^{water}$  and bulk water density  $\rho_{bulk}^{water}$ . The partitioning coefficient than independent on the size of the system and can be calculated by following

$$K = \int_{z_1}^{z_2} exp \left( \frac{-\Delta G(z)}{k_B T} - \frac{\rho_{(z)}^{water}}{\rho_{bulk}^{water}} \right) dz \times \frac{APL}{M_{lip} m_u}$$
 (7)

where APL stand for the area per lipid,  $M_{lip}$  is the molecular weight of lipids and  $m_u$  the atomic mass constant. The multiplication factor converts values of the partition coefficient into values directly comparable with experiments kg(lipid)/L(water). In contrary to permeability coefficient, the partitioning depends strongly on the negative values of the free energy.

In order to enumerate the permeability coefficients, the inhomogeneous solubility-diffusion model requires the calculation of local **diffusion coefficients** D(z). In enhanced sampling simulations, such as the umbrella sampling or the z-constraint method, molecules are constrained at given position along membrane normal, therefore their diffusion is restricted to the xy - plane.

The local diffusion coefficients are calculated by integrating the autocorrelation function (ACF) of the average constrained force acting on molecules as

$$D(z) = \frac{(k_B T)^2}{\int_0^\infty \langle ACF(F(z)) \rangle dt}$$
 (8)

where ACF(F(z)) is the autocorrelation function of the force on solute when constrained at position z along the axis. Similarly, the diffusion coefficient can be calculated from the velocity ACF or from the mean square displacement of the drug.

It is worth mentioning, that obtaining experimentally values for free energy of transfer  $\Delta G(z)$  or diffusion coefficients D(z) is not possible since there are no techniques capable of grasping such fine properties. In contrary, the partition coefficients are relatively easy to resolve by numerous experimental techniques, such as solid phase microextraction or equilibrium dialysis and are directly comparable to calculated ones. As for experimental permeabilities, the most straightforward approach is to measure diffusion (and consequently concentration) of drug between compartments (donor and acceptor) separated by thin film (skin graft), for example by Franz diffusion cell. Another *in vitro* approach is to use biological cell assays, like Parallel artificial membrane permeability assay (PAMPA<sup>25,26</sup>), or colorectal adenocarcinoma cells (Caco-2<sup>27</sup>) line cells. Unlike to simple partitioning, the permeability coefficients vary based on technique used and therefore are not suitable for a direct comparison with calculated permeabilities. Nevertheless, cautious comparison of calculated permeabilities based on the same methodology is generally acceptable.

#### 4. Membrane proteins

Membrane proteins (MPs) represent about a third of the proteins in living organisms and constitute about half of the total mass of biomembranes. They are responsible for processes occurring near the membrane interface or directly within the membrane based on the nature of protein-membrane interaction. Integral (intrinsic) membrane proteins are tightly bound to membrane structure by one (usually  $\alpha$ -helical anchor) or more membrane-spanning domains or attached via lipids. Those transmembrane segments are composed of conserved hydrophobic motives that interact directly with hydrophobic space within the membrane core. These types of proteins mediate the transport of molecules (membrane channels and transporters), energy transduction (charge translocating MPs) or catalytical processes (membrane-bound enzymes). On the other hand, peripheral (extrinsic) proteins are loosely bound to the membrane surface, and the dynamics between bound and unbound state can be shifted by changing the natural conditions, for example, by the concertation of the salt. Those proteins are usually water-soluble enzymes (like phospholipases), and the contact with biomembranes is omitted to interactions with lipid head groups.

Many membrane proteins are, by some means, associated with drugs – either by the mediation of membrane translocation or by their biotransformation – since processes involving drugs closely related to biomembranes. Among those, an important class of cytochrome P450 enzymes play special role in metabolism of many endobiotics and xenobiotics.

#### 4.1 Cytochrome P450 enzymes

Cytochrome P450 enzymes are a large superfamily of proteins found in animals, plants, fungi, protozoa, bacteria and even among viruses. Up to this day, more than 50,000 CYPs have been identified from which only 57 CYP genes from 17 families belong to humans. The pivotal role of this hemoprotein is the biotransformation of drugs and other xenobiotics.<sup>28</sup> They generally catalyze the biotransformation of hydrophobic substrate into more hydrophilic metabolite, that is rather easily eliminated from the organism. The mechanism of monooxygenase reaction underlying the catalytical activity of CYPs resides in the reduction of molecular oxygen into two atomic oxygens, with one atomic oxygen is then bound to aliphatic position of substrate molecule and the second oxygen atom is reduced to water by following scheme:

$$RH + O_2 + NADPH + H^+ \rightarrow ROH + H_2O + NADP^+$$
 (9)

where NADPH is the reduce form of nicotinamide adenine dinucleotide phosphate cofactor, RH is the aliphatic substrate and ROH the polar metabolite. The hydroxylation reaction itself is mediate by the heme cofactor buried within the center of the active site of CYP. The heme

cofactor is composed of the porphyrin ring with iron atom in its center. The heme-containing cavity of CYP is connected to protein surface via network of access and egress channels facilitating the transport of drug and its metabolite in and out the active site.

Despite relatively low sequential similarities (around 40%) among CYP families, the common fold of CYPs is highly conserved with predominantly  $\alpha$ -helical motives with small fraction of  $\beta$ -sheets. CYPs secondary structural features are denoted in alphabetical order starting from the N-terminal part of protein. The most important structural motives are the I-helix, contain threonine amino acid involved in catalytic cycle of heme, the F/G-loop connecting the F and G helices and the B/C loop connecting the B and C-helices. Those highly flexible loops are (together with F and F-helices) important in drug trafficking as they gate the path in and out of the active site of CYPs. (Figure 7 panel A)

In contrary to water soluble prokaryotic CYPs, eukaryotic CYPs are usually attached to membranes. Most of the mammalian CYPs are bound to the cytosolic side of the endoplasmic reticulum membrane or to the inner mitochondria membrane. This provides them the matrix for to mediation of substrate and product channeling in and out of the active site of the protein. Moreover, biomembranes facilitate the interactions of CYPs with redox partners and also the with another CYPs. In general motive of CYP-membrane association, the hydrophobic N-terminal anchor is incorporated within the membrane while the catalytical domain of CYP flows on the membrane surface. Here the proximal side of catalytical domain (defined by orientation of heme cofactor) faces the aqueous environment, while the distal side is partially immersed in membrane by F/G and B/C-loops, parts of F and G-helices and partially by  $\beta$ 4,  $\beta$ 5-sheets and  $\beta$ 4- $\beta$ 5 sheet (so called  $\beta$ -finger) (Figure 7 panel B). In this arrangement, the orientation of the distal side enables the interaction with redox partners.

The main distinguishing feature between microsomal and mitochondrial CYPs is the character of membrane interaction. Microsomal CYPs are synthesized by ribosomes directly bound to membranes rough ER and after translation are incorporated into the ER membrane. In contrary to that, mitochondrial CYPs are synthesized freely into cytoplasm and are post-translationally targeted to mitochondria via small leader sequence cleaved upon import. Compared to microsomal CYPs, cytochromes P450 found in mitochondria (like CYP11A1) are loosely associated with the inner mitochondrial membrane (IMM) since they lack the N-terminal anchor, and the interaction is omitted to specific segments of catalytical domain.

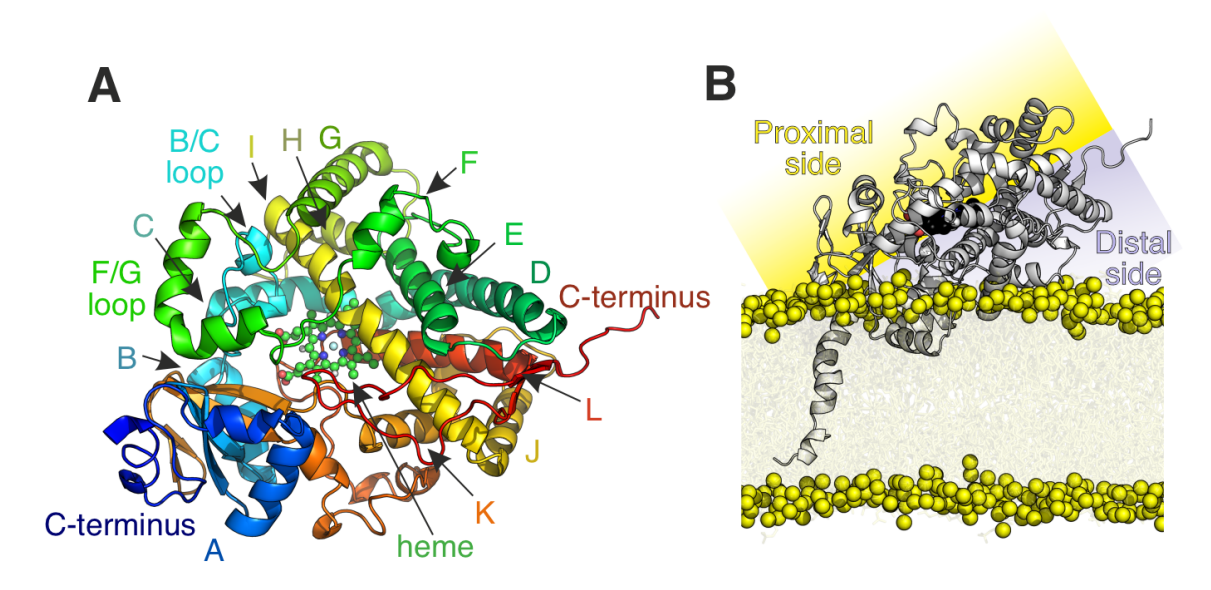


**Figure 7**. Structural features and membrane position of CYPs. The secondary structure of CYP with underlying individual protein segments denoted in alphabetical order starting from the N-terminal part of protein to C-terminal part (**A**). The orientation of CYPs on membrane surface (**B**). The N-terminal anchors the catalytical domain in membrane. The orientation of heme cofactors defines the proximal side (water facing) and the distal side (membrane facing) of the protein.

The immersion and overall orientation of CYP on the membrane depends on composition of membrane in which the protein is bound. The orientation of the catalytical domain can be determined from experimental measurements of the heme tilt angle (HTA). The heme tilt angle which is characterizes as the angle between plane of the heme cofactor and the membrane normal is widely used as benchmark for evaluation of MD simulations of membrane bound CYPs in comparison to spectroscopic measurements. The orientation of the CYP on the membrane is significantly affected by the lipid composition especially by the presence of charged lipid species originated from its head group substituent. For negatively charged lipid (like DOPG) CYPs show high inclination toward the membrane when compared to the neutral DOPC lipid. Also, the level of cholesterol content modulates the mutual CYP-membrane orientation as the HTA ranges from 52° to 68° (from pure membrane up to 50 wt% of cholesterol). The HTA values range from ~35° to 80° between different CYP isoforms.<sup>29</sup>

#### 4.2 Cytochrome P450 reductase

All mammalian CYPs rely on a supply of redox equivalents in form of electrons from its redox partners. To catalyze the monooxygenase reaction, CYP needs to obtain consequently two electrons, each at given step of the catalytic cycle. The electron transport chain is facilitated by cytochrome P450 reductases and cytochrome b<sub>5</sub> enzymes in microsomes and by ferredoxin redox systems in mitochondria. In microsomes both redox partners are located at cytosolic side of the ER with the CPR:CYP ratio of approximately 3-15:1.<sup>30</sup> Even small disruption of CPR function may lead to a major disruption of various CYP catalytic reactions. Such examples of close connection between CPR function and CYP activity decrease are found in cases of patients suffering Antley-Bixler syndrome. The deleterious mutations in CPR gene are responsible for lanosterol 14α-demethylase (CYP51) activity decrease previously observed in ABS patients.<sup>31</sup>

Human cytochrome P450 reductase is coded by a single gene located at chromosome 7qll.2 and contains 680 amino acids in its sequence.<sup>32</sup> CPR is diflavin reductase – contains both flavin adenine dinucleotide (FAD) and flavin mononucleotide (FMN) cofactors – attached to the ER membrane by N-terminal anchor while its flavin domains are facing the cytosol. CPR also bears NADPH cofactor that subsequently reduces flavin cofactors. The catalytical domain of CPR comprises of four subunits – two flavine binding domains coupled by the connecting linker domain and the NADPH binding domain at C-terminus. The FMN binding domain is connected to the linker by so called hinge. This highly flexible loop (unresolved in crystal structures) seems to be responsible for domain movement as it enables the pivoting of individual flavodomains (Figure 8).

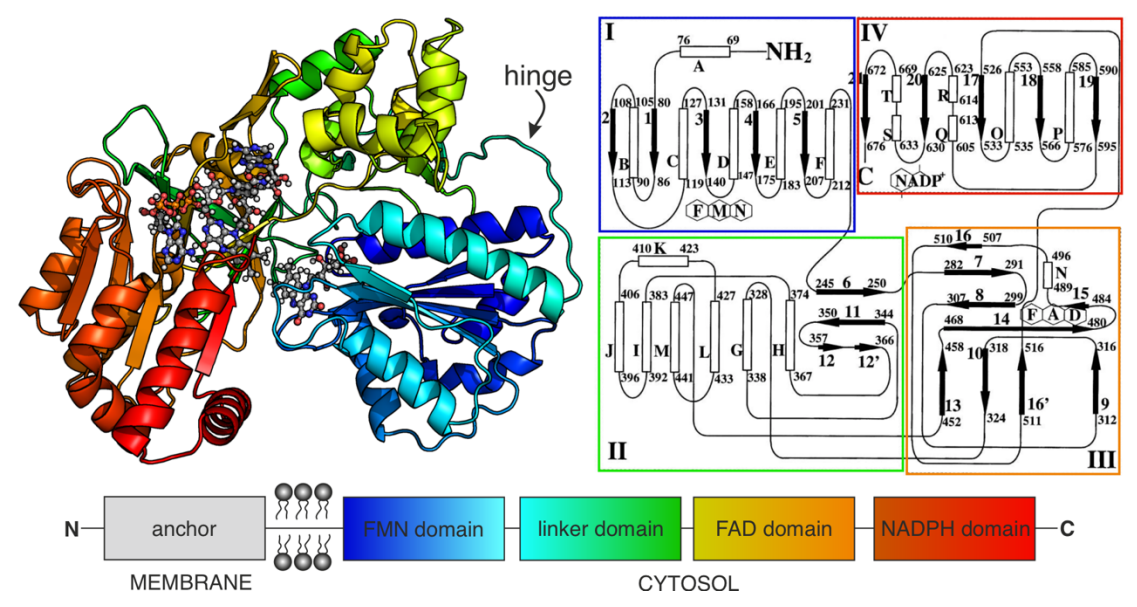


**Figure 8.** Basic structural features and topology diagram of CPR. Diflavin reductase is composed of 4 subdomains (cytosol facing) and N-terminal anchored (transmembrane part).

Based on the phase of the redox cycle, CPR can adopt two distinguishable conformations i.e., a closed or an open conformation. Multiple crystal structures of mammalian CPR in closed form are known, suggesting a compact and stable form, with flavin cofactors at close proximity (4 Å). At this conformation, all three cofactors are internally bound in a position allowing a cascade of intra-protein electron shuttling from NADPH to FAD and thereupon to FMN cofactor. The reduction of flavine cofactors then induces the CPR opening. Contrary to closed conformation, the open form is less compact with FMN and FAD cofactors being separated up to 86 Å apart (in case of yeast-human chimeric CPR). This leaves the FMN domain exposed to water environment clearly revealing the FMN cofactor. At this arrangement, CPR is compatible for the docking to its redox partner and for mediating the inter-protein electron transfer (Figure 9).

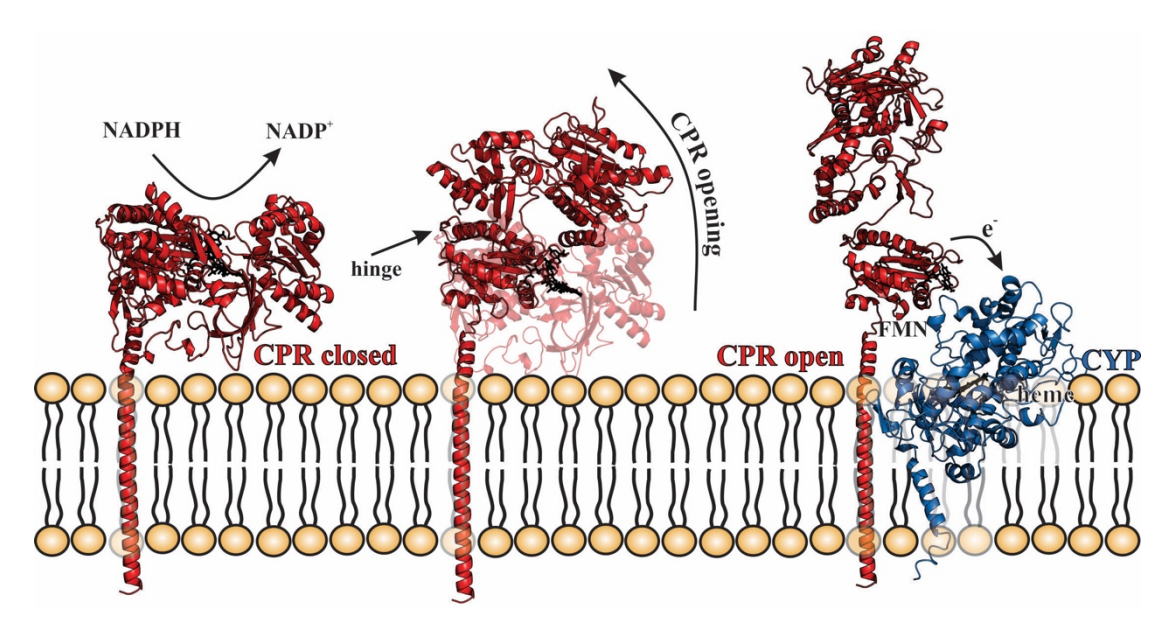


**Figure 9**. General scheme of CPR function. CPR is reduced by intra-cofactor electron cascade from NADPH cofactor. Upon CPR reduction, protein adopts more open conformation capable of enter-protein electron transfer towards its redox partner (CYP).

#### 5. Results

Following chapter summarizes our contributions to understanding and rationalization of how biomembranes interact with other biological species using different theoretical approaches.

The Results chapter is divided into five subchapters each dedicated to individual project and contains both, results published in peer-reviewed articles and not yet published papers and data. First subchapter describes the development and usage of MolMeDB database. Second subchapter is dedicated to an unpublished study on how cyclosporin A permeates through various of biological membrane models. Third subchapter refers to the development and validation of systematic computational methodology for prediction of suitable liposomal encapsulation for thermally induced release of bio-active compounds. Finally, two last subchapters describe the effect of membrane on behavior of the membrane-interacting proteins from superfamily of hemecontaining enzymes i.e. cytochromes P450s and its mutual interaction with redox partner CPR.

#### 5.1 MolMeDB project

Biomembranes are complex systems that serve as natural barriers for many compounds. They act on multiple levels within the human body – on cellular and sub-cellular level as well as on macroscopic scale, like skin barrier. At all those levels, the molecule-membrane interactions are important for the course of action of individual molecules in the organism and for their pharmacokinetics and pharmacodynamics. Multiple experimental techniques for assessing drugs partitioning (like SPME<sup>33,34</sup>) or permeabilities (Caco-2<sup>35</sup>, PAMPA<sup>36</sup>) were derived, providing us with large amount of data on how molecules interact with membranes. Furthermore, various databases like EDETOX<sup>37</sup> focused on in vitro and in vivo percutaneous permeabilities or PerMM database<sup>38</sup> using thermodynamics-based computational method to predict permeabilities through artificial and natural systems have been developed. Moreover, molecular dynamics simulations can provide complex information on both partitioning and permeability and on general behavior like orientation and favorable positions within membrane. MD-based methods generally focus on the effect of specific drug class or membranes. Finally, COSMO-based calculations represent and an accurate and relatively fast prediction of drug-membrane behavior suitable for high-throughput screening. All those data are not interlinked and scattered across multiple platforms and in literature, thus lacking thorough benchmark comparison among individual method/membrane systems.

To fill this gap, we have developed Molecules on Membrane database (MolMeDB) – an open chemistry database about interaction of molecules with membranes. Up to this day, MolMeDB contains more than 931,000 specific drug-membrane interactions for more than 456,000 unique molecules. Interaction data are linked directly to specific membrane system and technique – up to now database contains 41 membrane systems and 54 methods. (Figure 10) The membrane systems are further divided based on its localization within organism such brain, cell, eye, intestine, or skin membranes and based on the used approach e.g., theoretical models (like simple bilayers) or experimental systems (complex cell lines like Calu-3 or Caco-2). Similarly, methods are divided based on the source of interaction data e.g., experimentally obtained, computed/calculated (QSARs, COSMO-based calculations) or simulated (MD-based techniques at different level of approximation).

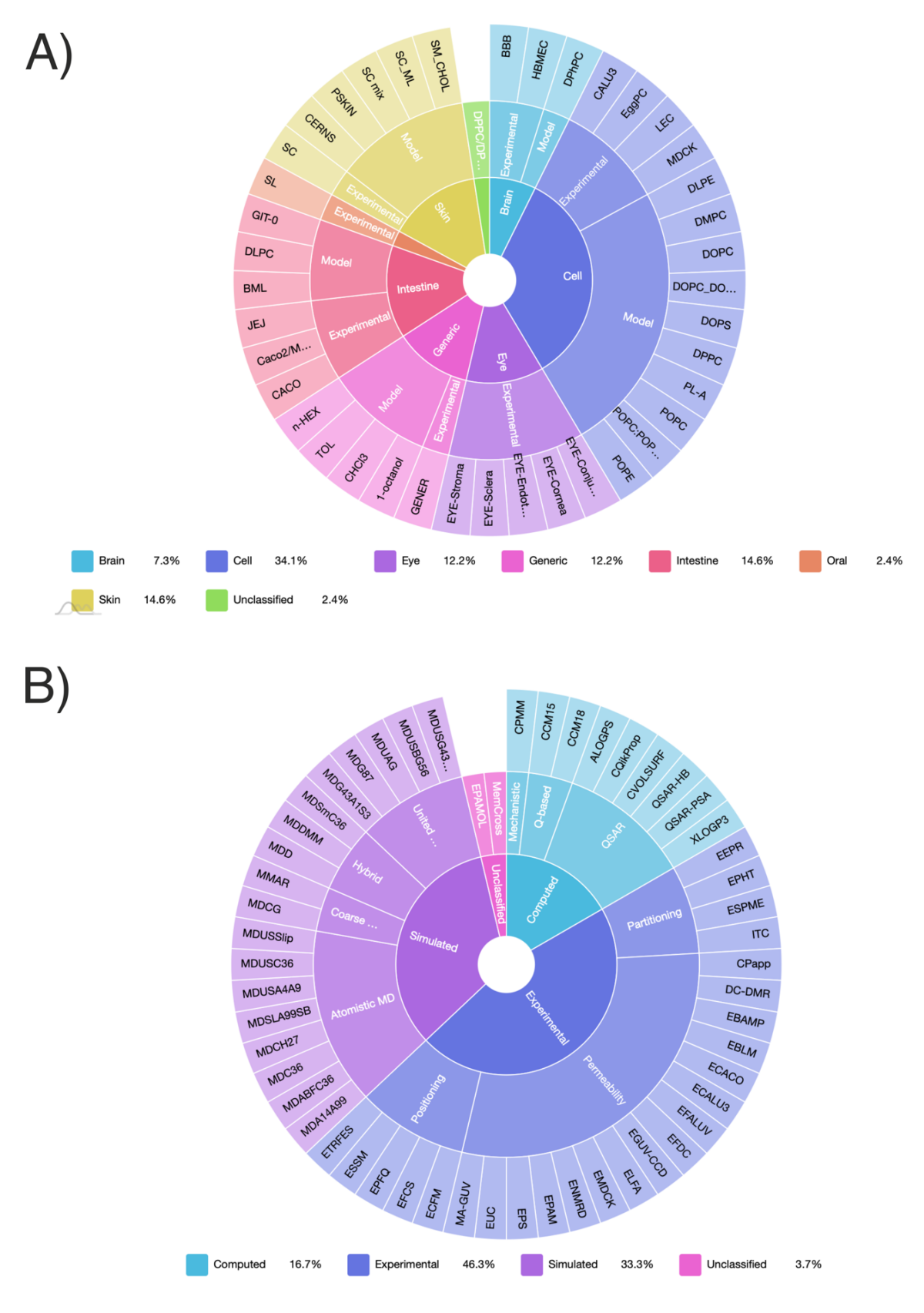


Figure 10. Distribution of total membranes (A) techniques (B) found in MolMeDB database.

It is worth mentioning that the latest version of MolMeDB also includes new information on membrane transporters and its interaction with small molecules. Especially on their relations to compound in terms of substrate or inhibitory/non-inhibitory effect.

#### 5.1.1. MolMeDB user interface

Web version of MolMeDB database is accessible (<a href="https://molmedb.upol.cz/">https://molmedb.upol.cz/</a>) and provides a user-friendly interface. Interaction data are accessible via Browse or Search mode, where user can either browse through lists of compounds that appertain to specific membranes and techniques or to directly search for desired compound by its name or SMILES notation. Upon choosing the entry a page for individual compound contains four sections:

- 1. **General info** provides a description of basic molecular properties like molecular weight, octanol/water partition coefficient predicted from RDkit software<sup>39</sup> or standard chemical identifiers and notations (InChiKey, SMILES). Moreover, it directly visualizes 2D and 3D structure of molecule. This section contains links to other databases like PubChem<sup>40</sup>, DrugBank<sup>41</sup>, ChEBI<sup>42</sup>, ChEMBL<sup>43</sup> or Protein Data Bank<sup>44</sup>.
- 2. **Interactions** displays an interactive table of all interactions available for a selected compound. For a given membrane-method combination is lists interactions such as membrane/water partition coefficient (log $K_m$ ), permeability coefficient (log $P_{erm}$ ), the height of the penetration barriers ( $\Delta G_{PEN}$ ), the affinity of drugs towards the membrane ( $\Delta G_{WAT}$ ) or the position of the interaction minima ( $\Delta Z_{MIN}$ ). It also contains the charge of the molecule (Q), temperature and link to reference publication from which data were obtained.
- 3. **Transporters** provides information about transporters and its interactions with compounds found on the database. It shows a targeted transporter with a link to UniProt database as well as characteristic constants such as half maximal effective concentration (pEC $_{50}$ ), half maximal inhibitory concentration (pIC $_{50}$ ), inhibition constant (pK $_{i}$ ) an Michaelis constant (pK $_{m}$ ). It also classifies the nature of interaction towards transporter as substrate, inhibitor, or non-inhibitor.
- 4. Free energy graph demonstrates free energy profiles of molecule-membrane crossing with respect to membrane normal between the membrane center (0 nm) and water environment (3.5 nm). At any given membrane depth (blocks separated by 0.1 nm) the free energy value can be interactively visualized.

#### 5.1.2. Case study

Multiple free energy profiles can be visualized together allowing the user to denote the effect of specific membrane/method on permeation of specific molecule or to compare multiple compounds on one specific membrane/method system setup. Both, interaction data and free energy profiles can be directly export in .csv format. The following case studies demonstrate the usage of the MolMeDB database.

#### Caffeine and its metabolites

Here the example of comparison of free energy profiles for caffeine and its derivatives shows the effect of different type of metabolizing reaction on metabolites permeation with respect to unmetabolized substrate (Figure 11). Caffeine is metabolized by various of metabolizing enzymes into following metabolites – theobromine (CYP1A2, CYP2E1), theophylline (CYP1A2, CYP2E1), 1,3,7-trimethyluric acid (xanthine oxidase), 6-amino-5(N-formylmethylamino)-1,3-dimethyluracil (CYP1A2) and paraxanthine (CYP1A2). The type of metabolizing reaction (demethylation, oxidation or decyclization) defines the chemical modification of resulting products. Free energy profiles showed distinguishable differences for individual metabolites with respect to caffeine substrate molecule. Demethylation reaction showed increase of the penetration barrier by  $\sim$ 3.4 kcal/mol for theobromine, theophylline and paraxanthine. Products of oxidation and oxidation/decyclization reactions displayed additional increase of penetration barriers with respect to caffeine by 5.4 and 5.9 kcal/mol, respectively. The most discernible increase of the penetration barrier was observed in the aliphatic tail region membrane while the affinity towards the membrane ( $\Delta G_{WAT}$ ) defined as the height of the membrane/water barrier remained almost unchanged for all molecules.

#### **Comparison of methods**

This case study shows bigger datasets (101 compounds) that allows the comparison of multiple membrane/method entries. Here we demonstrated the evaluation of theoretical methods against experimentally obtained data (Figure 12). Permeability coefficients obtained from two different theoretical approaches COSMOmic/COSMOperm18 calculations and PerMM predictions were evaluated against black lipid membrane (BLM) experimental setup. In COSMO-based calculations model of DOPC lipid bilayer was used while in BLM setup and PerMM predictions the permeabilities were determined on generic phosphatidylcholine membrane. Linear regression fit was employed to identify the level of correlation between the combination of two methods. The resulted coefficient of determination (R<sup>2</sup>) of 0.76 and 0.77 for COM18/BLM and PerMM/BLM, respectively presented good agreement of both theoretical approaches compared to experiment.

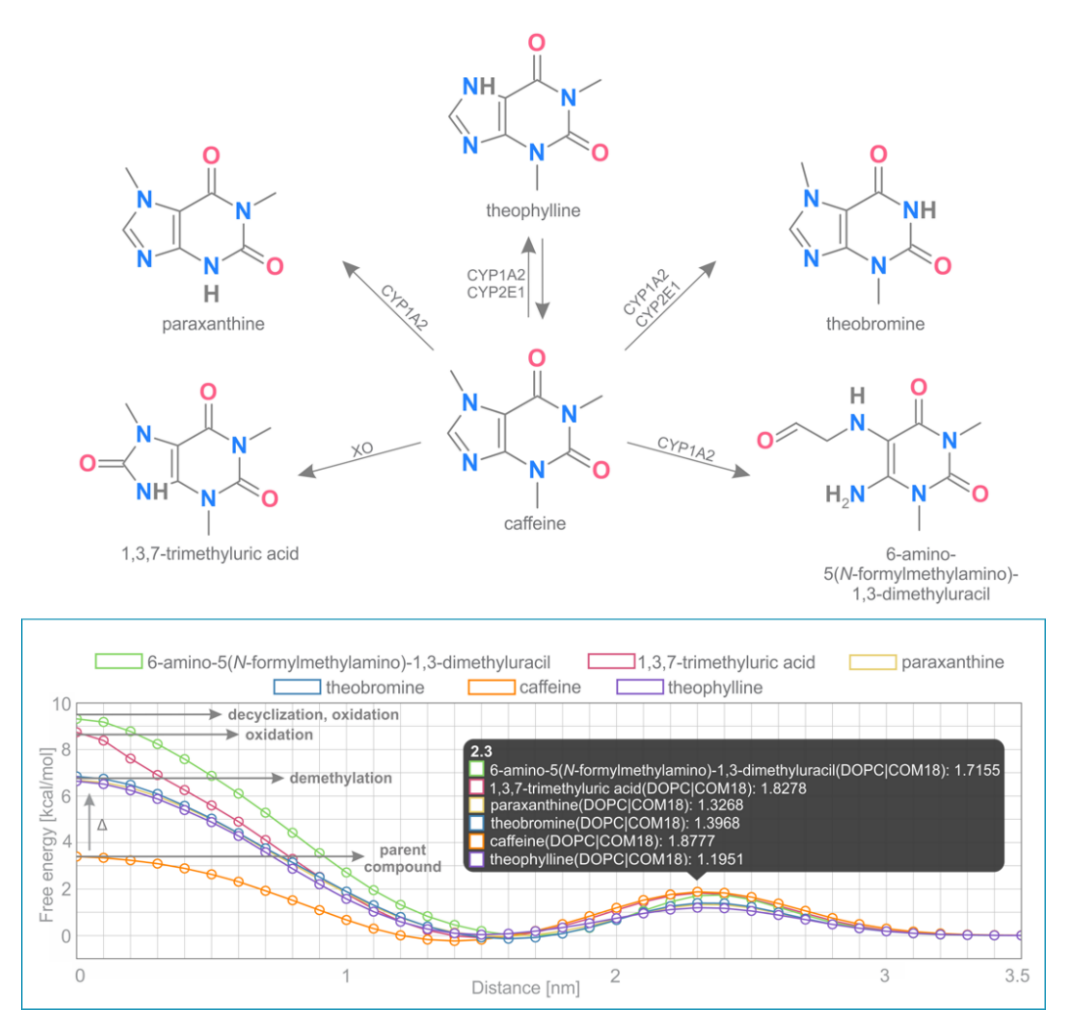


**Figure 11.** Free energy profiles of caffeine and caffeine metabolites permeation through DOPC membrane calculated with COSMOmic18 as example of MolMeDB usage. Structures of individual molecules are depicted along with enzymes responsible for caffeine metabolism. Figure taken from reference<sup>45</sup>.

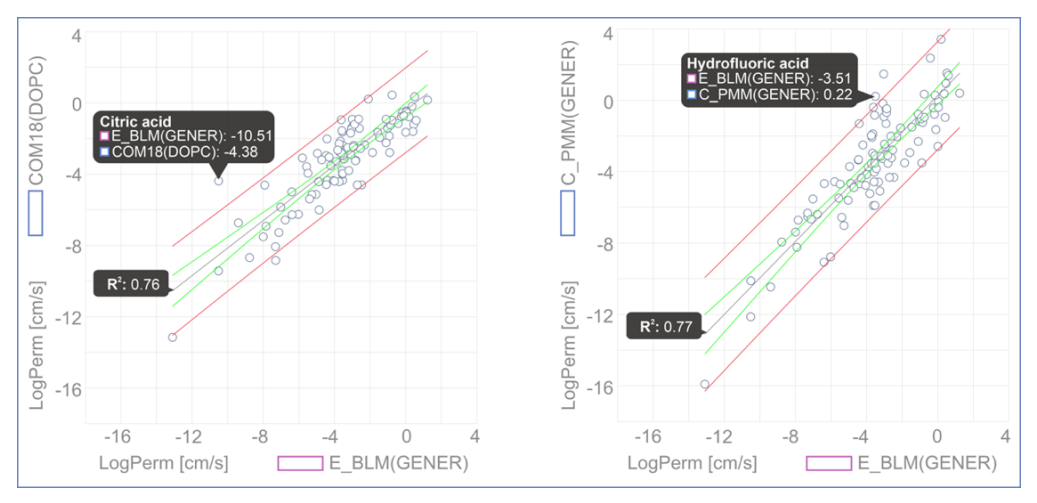


**Figure 12.** Comparison of permeability coefficients obtained from theoretical PerMM model, COSMO-based calculations against experimental BLM setup. The coefficients of determination and for COM18/BLM (0.76) and PerMM/BLM (0.77) along with almost identical slope to experimental data showed good correlation of between individual techniques. Prediction interval shown in green and confidence interval set to 95% shown in red. Figure taken from reference<sup>45</sup>.

#### 5.2 Permeation of cyclosporin A through biomembranes

Many naturally occurring cyclopeptides have been promising alternatives to traditional small drug exceeding beyond the rule of five (bRo5) space. Exceptional biological activity and the possibility of engineering their chemical structure to alter specific target response made them highly anticipated candidates in novel drug research. Contrary to traditional small molecules, peptides are biodegradable back to simple amino acid making them less toxic and fast removal upon proteolytic degradation restricts their accumulation in organs. On the other hand, the low oral bioavailability of cyclic peptides is limiting step in drug administration. One of the most prominent members of cyclopeptide family is cyclosporin A, widely used immunosuppressant, that possesses both membrane permeability and good oral bioavailability properties.

Cyclosporin A is an important immunosuppressant drug. In complex with cyclophilin A, CsA is bounds to calcineurin, calcium/calmodulin-dependent serine/threonine protein phosphatase responsible for dephosphorylation T-cells transcription factors. This ternary complex then specifically targets T-cells signaling pathways restricting the transcription and proliferation of T-lymphocytes (e.g. T-lymphocytes activation).<sup>47</sup>

From the structural point of view cyclosporin A is a homodetic cyclopeptide composed of 11 amino acids, where 7 nitrogen atoms are N-methylated (Figure 13). Cyclosporin A exhibits structural polymorphism, with two predominant conformations based on surrounding environments e.g. free form of CsA in non-polar solution and bound form in cyclophilin complex. In non-polar medium CsA adopts more "closed" conformation resulting four intramolecular hydrogen bonds and formation of antiparallel  $\beta$ -sheet. In contrary to that, while bound in complex with cyclophilin A in water, polar moieties of CsA are more exposed to maximize possible hydrogen bonding to protein and polar environment. This structural flexibility is crucial for membrane permeability of CsA.

After oral administration up to the point of reaching side of action, CsA permeates through various biomembranes differing in lipid composition and phase state. Specific interactions of CsA with individual inhomogeneous environment along with specific CsA physicochemical and structural properties (high hydrophobicity, low aqueous solubility, or N-methylated peptide backbone) underline the nature of distinct permeation process. Due to the hydrophobic character and limited water solubility suggested CsA is located primary in aliphatic membrane interior.<sup>52</sup> In fully saturated phospholipids (namely DPPC) the presence of CsA affects the ordering of acyl chains according to phase state e.g. increase in ordering above phase temperature and decrease of lipid ordering bellow transition temperature as well as decreases the enthalpy of transition from gel to

liquid crystalline phase.<sup>52,53</sup> The partitioning of between both gell and liquid crystalline phase is governed by the amount of CsA present in mixture.<sup>53</sup> Furthermore, the topology of membrane is changed by CsA partitioning into regions separating gel and liquid phases in cholesterol enriched membrane mixtures.<sup>54</sup>

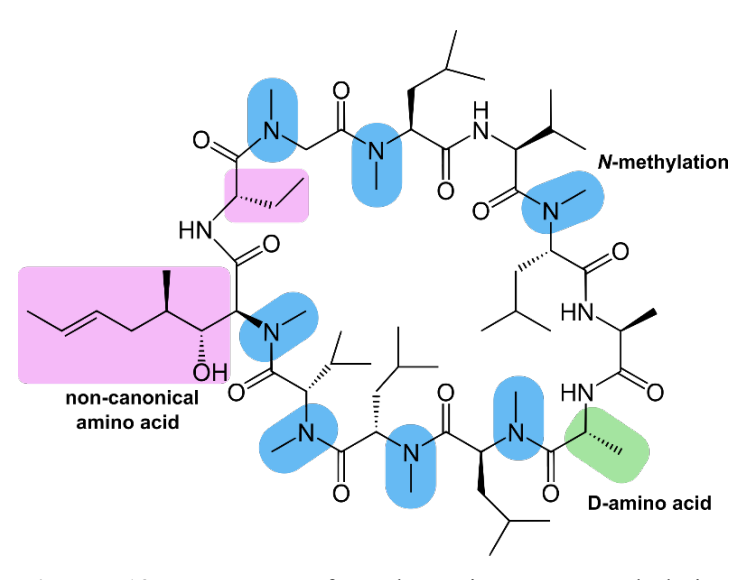


**Figure 13**. Structure of cyclosporin A. *N*-methylation sides highlighted in blue, two non-proteigeneric amino acids highlighted in pink, D-alanine highlighted in green. Adopted from reference.<sup>55</sup>

In present study, we describe the effect of different membrane composition of CsA permeation. We used enhanced umbrella sampling technique to investigate energetical profiles of CsA passage along membrane normal. In order to investigate the structural behaviour of CsA, we first carried out simulations in water and hexane.

In simulations of CsA in water and hexane the drug adopts two different conformational states as structural response to different environments. Measured "hydrophobic distances" – distances between COM of hydrophobic side chain residues and COM of whole CsA - (Figure 14. left) showed tighter packing of hydrophobic residues of CsA in hexane. In contrast to that, while CsA was in water, the hydrophobic moieties had greater conformation freedom, maximizing the interactions with surrounding water molecules. Furthermore, the native contacts between hydrophobic side chain residues and the rest of the molecule were measured (Figure 14. middle). The total amount of contacts was greater in simulation of hexane suggesting the effort to maximize the intramolecular contacts within CsA. This led to structural changes in CsA and exposing the more polar backbone of peptide while shielding the hydrophobic moieties within. Moreover, solvent accessible surface area (SASA) showed smaller area occupied by CsA in presence of hexane (Figure 14. right) as solvent also suggesting tighter packing in CsA molecule structure.

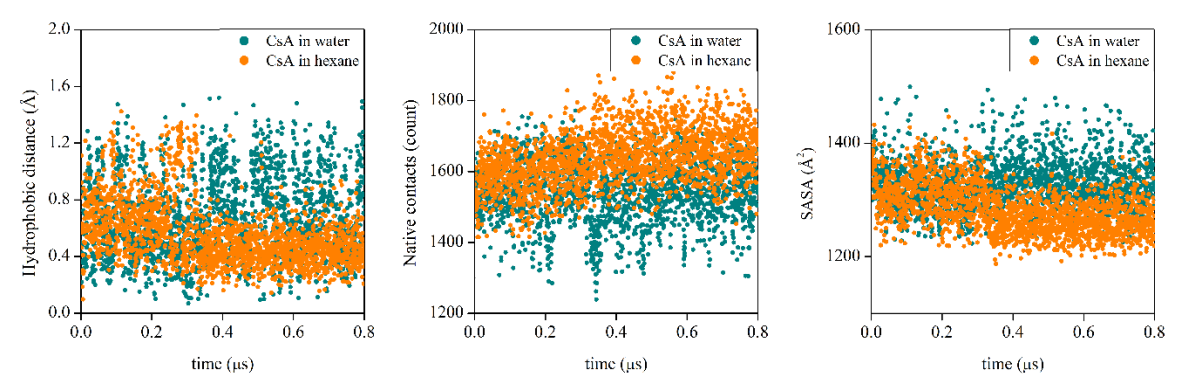


**Figure 14.** Different behavior of CsA in simple conditions e.g., in water and in hexane. In hexane CsA exhibited "closed" conformation while maximizing the intramolecular interactions. In contrary to that, the overall molecular surface was greater for CsA placed in water suggesting preferential interaction with water environment upon adopting "open" conformation.

Table 1. Energetical properties of cyclosporin A permeation in various membrane models

Membrane composition	$z_{min} \left[ \mathring{A} \right]$	ΔG <sub>WAT</sub> [kcal/mol]	ΔG <sub>PEN</sub> [kcal/mol]
DOPC	12.55	-8.15	4.00
DPPC	0	-30.44	0
DMPC	6.45	-10.00	3.05
POPE	9.55	-6.42	3.80
POPC	9.35	-11.75	4.14
POPC:CHOL (1:1)	3.25	-16.37	0.40
POPC:CHOL (4:1)	10.35	-8.06	5.20
POPC:POPE (1:1)	6.75	-9.36	3.62
POPC:POPE:CHOL (2:1:1)	11.05	-7.51	4.14

As the strongly hydrophobic character and limited water solubility suggested CsA is located primary in aliphatic membrane interior.

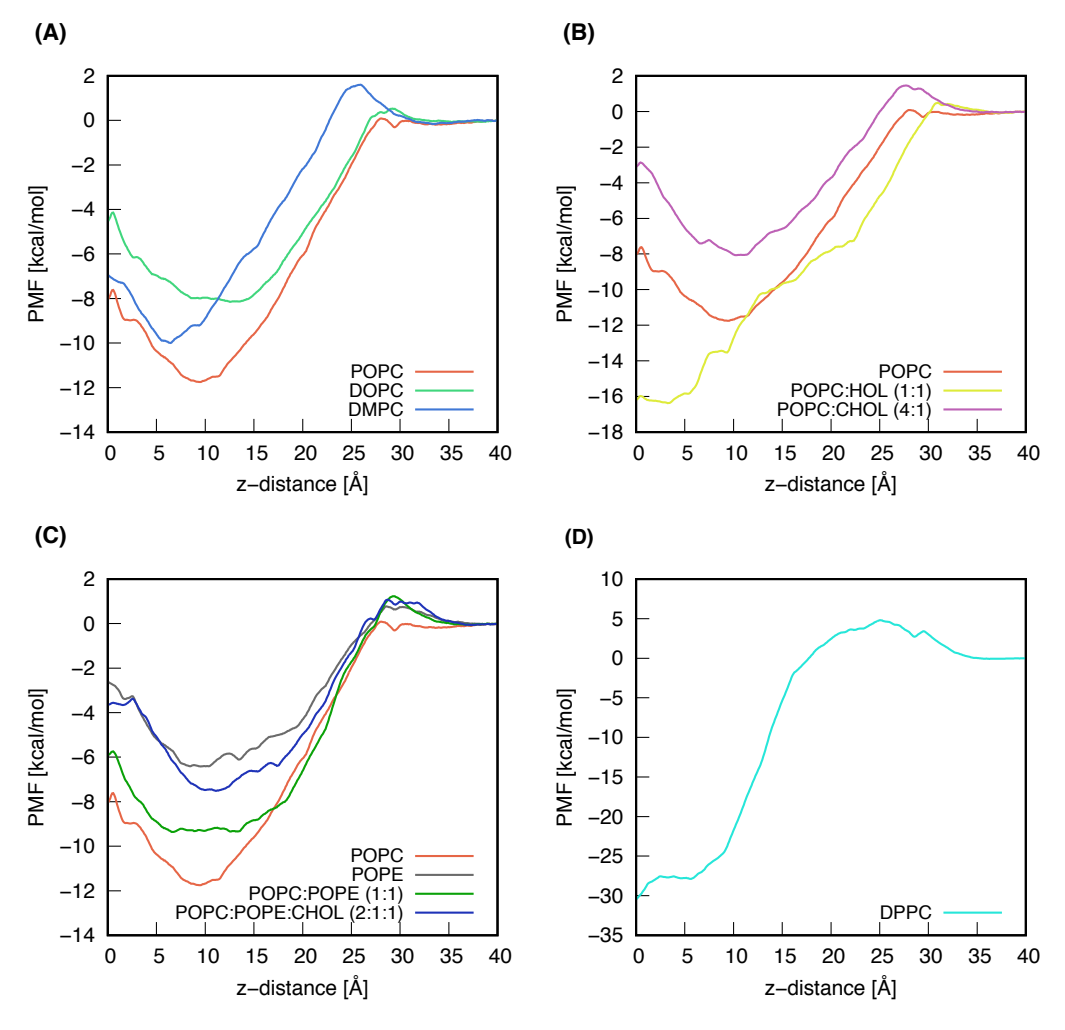


**Figure 15.** Calculated free energy profiles of CsA membrane permeation divided into four groups based on membrane composition. CsA passing through membrane starting at bilayer center (z=0) to water (z=40). **(A)** PMF profiles of CsA permeation through pure phosphatidylcholines membranes. **(B)** PMF profiles of pure POPC and analogues with different cholesterol amount. **(C)** PMF profiles of pure POPC, POPE membranes and its cholesterol enriched content. **(D)** PMF profile of CsA passing through DPPC bilayer found in gel ordered phase.

#### 5.2.1 Cyclosporin A behavior on membrane models

Phosphatidylcholines (PC) are one of the most abundant phospholipids in mammalian cell membranes most likely to be involved in passage of small molecules. Three prominent member of PC lipids were selected (POPC, DOPC and DMPC) differing in length and saturation of acyl chains. In case of POPC and DOPC, where the only differentiating factor is saturation in  $\Delta 9$ -cis bond, the PMF profiles show different position of energetical minima slightly shifted towards region of double bonds in case of DOPC (12.55 Å). The energy minima decreased by  $\sim 3.5$  kcal/mol in case of POPC. Nevertheless, the energy required for CsA to cross those membranes ( $\Delta G_{WAT}$ ) was almost the same. In case of DMPC the position of minima and the initial barrier for entering the membrane was shifted towards core due to the shorter length of acyl chains (Figure 15 A).

Second group considers case of pure POPC and its analogues with increasing amount of cholesterol content (POPC:CHOL (4:1; 1:1)). In case of pure POPC bilayer and system with lower saturation of cholesterol the energetical minima reside within same the position (~10 Å) from membrane center. In equimolar amount of POPC and cholesterol higher membrane ordering resulted into displacement of bilayer leaflets and shift of CsA energetical minima directly to the center of membrane which is the only disordered region. Once in the middle of membrane it is unlikely for CsA to overcome barrier of 16.37 kcal/mol (Figure 15 B).

In the third group the effect of changes in the polar headgroups was studied in prototypical types of lipids e.g. POPC, POPE. The most apparent difference of CsA permeation was the deepening of energetical minima by  $\sim 5.33$  kcal/mol while changing from PE to PC headgroup ( $\Delta G_{WAT}$  -6.42 and -11.75 for POPE and POPC respectively) while the position of energetical minima was almost the same. Subsequently, while in equimolar composition of POPC and POPE lipids the energetical barrier of crossing showed average between POPC and POPE ( $\Delta G_{WAT}$  -9.36) the PMF profile showed significant bordering of energetical minima oscillating from 6 to 14 Å. As showed in previous case, additional increase of cholesterol content affected negatively the partitioning of CsA into membrane (Figure 15 C).

Extreme case of CsA crossing DPPC membrane found in gel ordered phase. In contrary to other systems PMF profile shows significant barrier for entering membrane from water environment  $\sim$ 5 kcal/mol. Once penetration beyond headgroup region CsA finds its minima in the center of the membrane with  $\Delta G_{WAT}$  of -30.44 kcal/mol where it will reside (Figure 15 D).

#### 5.2.2 Conclusions on cyclosporin A

In simplified phosphatidylcholine membrane models, the energetical profiles for CsA passage were relatively similar. However, the presence of cholesterol induced changes in the membrane's ordering, leading to a shift of the energetical minima directly towards the center of the lipid bilayer when equimolar concentrations of cholesterol and phosphatidylcholine were present. The borderline case of DPPC also revealed that CsA was unable to permeate through membranes in the gel-ordered phase. In all cases, the strongly hydrophobic nature of CsA and its limited water solubility indicated that CsA primarily resides within the aliphatic interior of the membrane. These findings shed light on the importance of membrane composition in influencing the permeation behavior of CsA and highlight the preferential localization of CsA within the lipid bilayer.

## 5.3 *In silico* screening of drug candidates for temperature-responsive liposome formulation

Liposomes are spherical vesicles which comprises of aqueous core surrounded by a lipidic shell arranged in form of bilayer. The lipidic part of liposomes usually contains various of phospholipids and cholesterol. Upon initial encapsulation into internal cavity, liposomes as are used as carriers for large numerous active substances such active pharmaceutical ingredients (APIs), fluorescent dyes or genes. The properties of liposomal vehicles such as size, stability, and composition can be specifically altered for the purpose of desired delivery and release mechanism. The precise tailoring of the composition of lipid species may also affect the one of the key properties for successful payload release e. g. the permeability of encapsulated compounds. At lower temperatures lipid bilayers tend to reside in order phase which is non-permeable for trapped species and is desired for sufficient transport of encapsulated compounds towards their side of the action. On the other hand, when heated, the phase transition of lipid bilayers into disordered state must assure the controlled release of encapsulated species. The phase properties of lipid bilayers are to the greatest extent govern by the composition of lipidic part of the liposomes.

Up to this day, liposomal formulation and the encapsulation-release mechanism faces many drawbacks originating from the non-systematic ways of determining the correct formulation approaches or the appropriate identification pharmaceutical ingredients suitable for encapsulation. The goal of the present work was to develop and validate a systematic computational methodology for prediction of suitable encapsulation and thermally induced release of bio-active compounds. The proposed strategy combined classical molecular dynamics simulations and quantum chemistry-based calculations to determine selection criteria for identification of compounds capable of stable in encapsulation and temperature-induced release from liposomes on well-established membrane model (membrane composed of DPPC:DPPG:CHOL at molar ratio of 75:10:15). Those criteria were validated against series of experiments confirming the methodology precision using an identical set of fluorescent dyes. Furthermore, we screened the DrugBank database against those criteria and successfully identified potent drug – cycloserine – capable of liposomal loading ant thermal release.

#### 5.3.1. MD simulation of bilayer phase transition

Molecular dynamics simulations of mixed membrane (DPPC:DPPG:CHOL at molar ration of 75:10:15) were carried out at scale of temperatures mimicking different stages of liposomal formation a subsequent cargo release – the liposome storage temperature (293 K), slightly elevated body temperature (313 K) and the temperature desired for the controlled release of trapped payload (323 K and 333 K). At the temperature corresponding to liposomal storage (293 K) and body temperature (313 K) the bilayers were found at highly ordered state. Sharp changes in bilayer structural features (A<sub>L</sub> increase by approximately 1 nm<sup>2</sup> and lower order parameters marked the phase shift into disordered state between 323 K and 333 K. At the temperature of 333 K, required for the cargo release, lipid bilayer was found in completely disordered state. Structures from abovementioned MD simulations served as templates for following COSMOmic/COSMOperm calculations.

# 5.3.2. COSMO-based partitioning and permeability calculations fort fluorescent dyes

Set of five fluorescent dyes was used as starting set for derivation of encapsulation/release selection criteria – namely 5-carboxyflourescein (5-CF), 6-carboxyflourescein (6-CF), fluorescein (F), fluorescein-5-isothiocyanate (FITC) and calcein (Cal). For each fluorescent dye/bilayer system partitioning and permeability coefficients were calculated at given temperature range (Figure 20). The temperature dependent calculations showed no significant changes in partitioning of fluorescent dyes into mixed membrane (Figure 16 panel A). Only at elevated temperature (333 K) slight inclination to increase of partitioning was manifested. From the partitioning coefficients the lipophilicity of individual compounds could be assessed as follows Cal < 6-CF < 5-CF < F < FITC. On the contrary, the permeabilities of studied dyes increased almost linearly with increasing temperature (Figure 16 panel B). Those differences varied widely also between individual compounds. The further analysis of partitioning and permeability coefficient at limited temperatures (293 K and 333 K) suggested the 5carboxyflourescein and 6-carboxyflourescein as the best candidates for thermoresponsive release as they would prefer aqueous cavity ( $log K_{lip/wat}^{293K} = 0.72 \pm 0.43$  and  $0.35 \pm 0.36$  for 5-CF and 6-CF, respectively) and would not escape from the liposome core rapidly ( $logP_{erm}^{293K} = -5.64 \pm$ 0.06 and  $-5.78 \pm 0.06$  for 5-CF and 6-CF, respectively) In contrary to that, higher permeability coefficients for fluorescein ( $log P_{erm}^{293K} = -2.59 \pm 0.09$ ) and fluorescein-5-isothiocyanate  $(log P_{erm}^{293K} = -2.26 \pm 0.52)$  would suggest higher than optimal permeability even at lower temperatures. Moreover, the lowest permeability even at higher temperatures for calcein  $(log P_{erm}^{333K} = -9.05)$  denotes its inability to escape from aqueous core of liposome.

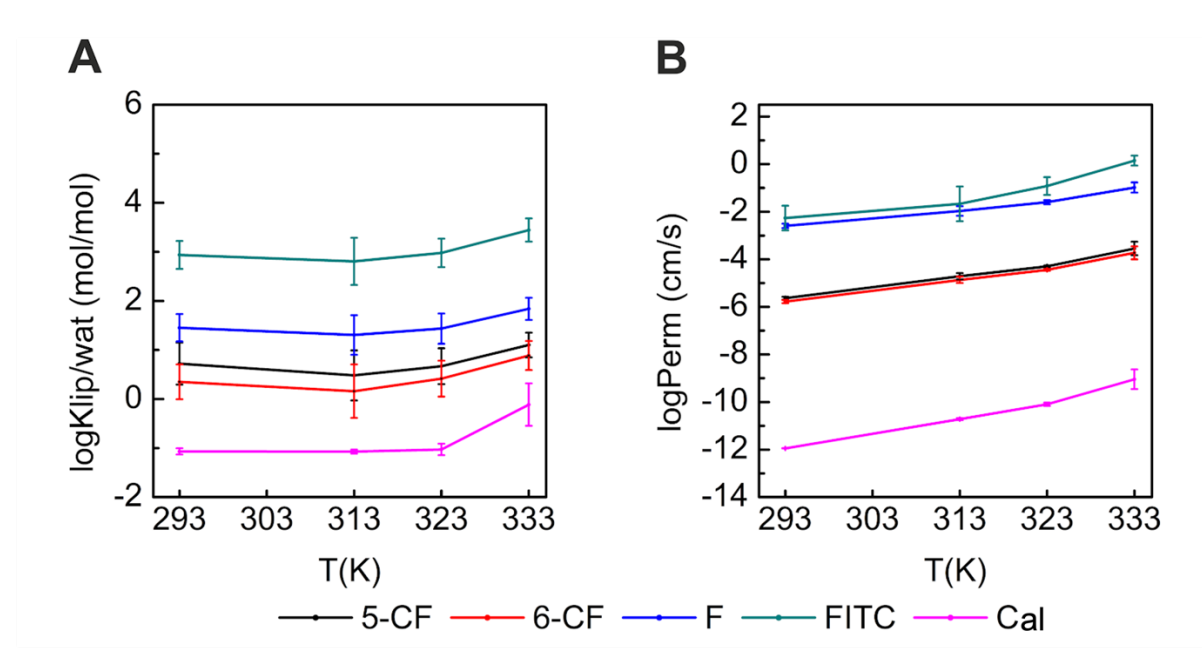


**Figure 16**. Calculated partitioning (**A**) and permeability (**B**) coefficients for the set of fluorescent dyes through mixed membrane (DPPC:DPPG:CHOL at molar ratio of 75:10:15).

## 5.3.3. Selection criteria encapsulation/thermoresponsive release and DrugBank screening

Based on theoretically calculated partitioning and permeability coefficient and encapsulation and released experiments with fluorescent dyes we derived set of ground criteria for prediction of successful encapsulation/thermoresponsive release (Figure 17) liposomal DPPC:DPPG:CHOL (75:10:15) membrane mixture. From the experimental point of view, adjustments were made to reflect real experimental conditions. For example, the boundary of partitioning coefficients was shifted to reflect the equal contribution of volumes of lipidic part/aqueous phase of liposomes (lipids tend to occupy 100 - 10,000x less volume compared to aqueous core) which resulted at the rule  $logK_{lip/wat} < 2$  (rather than 0) for optimal encapsulation into aqueous cavity. The border values for permeability coefficients were recalculated into apparent permeabilities to reflect the fraction of unionized species and correction to unstirred water layer. The apparent permeabilities at given temperatures of 293 K and 333 K (logP<sub>app</sub><sup>293K</sup>) outlined boundaries for optimal temperature controlled released as logP<sub>erm</sub> < -9.1 at lower temperatures (273 K) and logP<sub>erm</sub> > -8.1 at release trigger temperature (333 K). Based on these rules (Figure 21), neutral molecules can be sorted into following categories:

i/ compound are not suitable for liposomal encapsulation

ii/ compound are suitable for liposomal encapsulation but are not suitable for the thermally controlled release

iii/ compound are suitable for liposomal encapsulation and for the thermally controlled release.

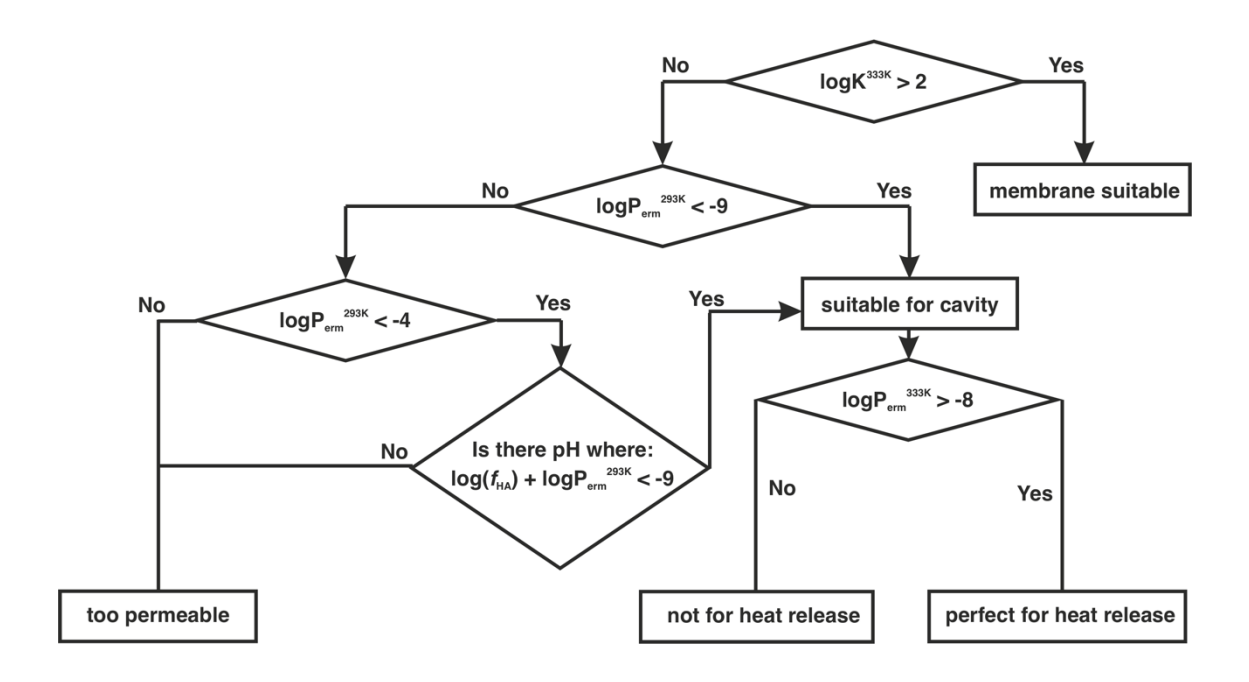


**Figure 17**. Selection criteria defining the optimal molecule candidates for successful liposomal encapsulation and subsequent release at trigger temperature.

To further validate those selection criteria, we performed rapid *in silico* screening of compounds found in DrugBank database. In total of 56 bioactive (mostly toxic) compounds were selected for which their  $logK_{lip/wat}$  and  $logP_{erm}$  values were calculated. From abovementioned selection criteria those 56 compounds were high divided into three categories:

i/ 27 compounds would encapsulate rapidly into membrane phase of the liposomes due to their high partitioning coefficients (Figure 18. yellow dots) and 4 compounds were not acceptable for liposomal formulation using the Bangham approach (low permeability even at higher temperature of 333 K; Figure 18. red dots)

ii/ 16 compounds were not acceptable for liposomal formulation as they were classified as too permeable (Figure 18. black dots).

iii/ 9 compounds were classified as potential candidates for both suitable liposomal encapsulation and thermally controlled release (Figure 18. blue dots).

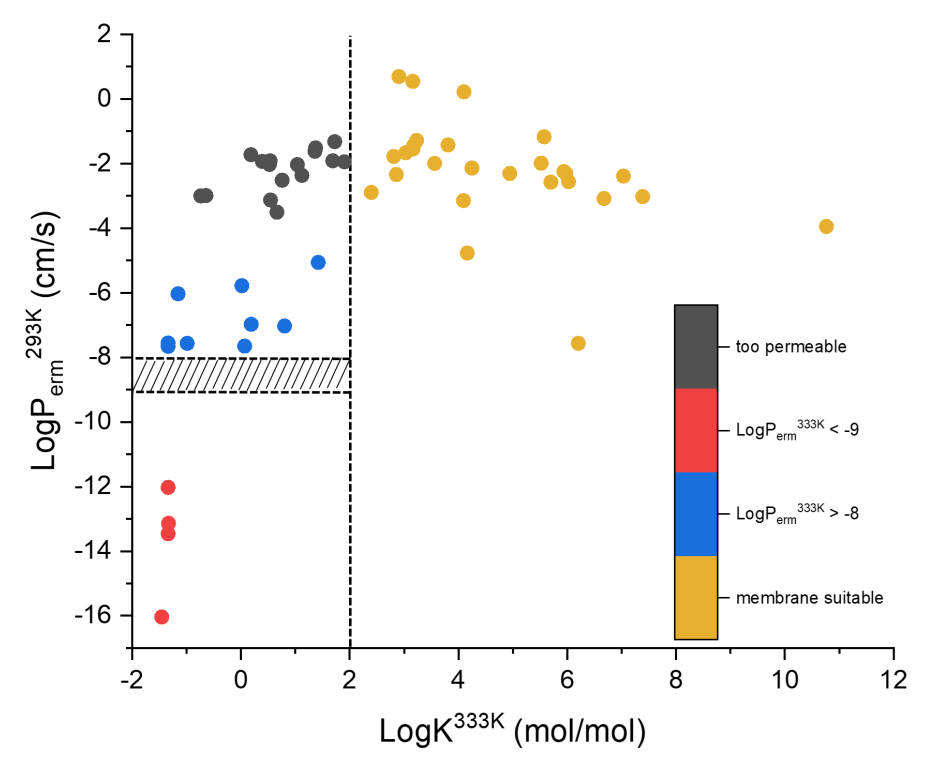


**Figure 18**. Classification of 56 toxic compounds into categories database based on selection criteria. Almost half of selected drugs would reside predominantly in the membrane phase rather than in the aqueous environment (yellow dots). Another 20 compounds were classified as either too permeable (black dots) or as almost not permeable even at higher temperatures (red dots) and therefore not suitable for controlled release. The remaining 9 compound met both selection criteria for feasible entrapment into aqueous phase and consequent release at desired temperature (blue dots).

Furthermore, out of those 9 possible candidates cycloserine (bioactive compound with antibacterial properties) was chosen for liposomal formulation experiment. After liposomal encapsulation the stability of originated liposomes at both storage and release temperatures was tested on measuring the proliferation of E.coli bacteria on the resazurin assay. Estimated apparent permeabilities confirmed the ability of cycloserine to permeate at elevated temperatures (logP<sub>app</sub><sup>333K</sup> = -8.66) while not being prematurely released from liposome at lower temperatures (logP<sub>app</sub><sup>273K</sup> = -10.1).

### 5.4 Behavior of Mitochondrial Cytochrome P450 11A1 on DOPC and Mitochondrial Membrane Models

The mitochondrial cytochrome P450s are enzymes involved in the biotransformation of many compounds predominantly secreted from the adrenals and gonads.<sup>56</sup> One of the most important processes mediated by mitochondrial CYPs is steroidogenesis that leads to the production of steroid hormones responsible for the regulation of metabolism, balance of energy or responses to stress.<sup>57</sup> The steroidogenesis in mitochondrion is mediated by cytochromes P450 from family 11 – CYP11A1, CY11B1 and CYP11B2 which all contain mitochondrial targeting sequence affecting their cellular specificity.<sup>57</sup> Cytochrome P450 11A1 (CYP11A1), also known as P450scc (side-chain cleavage enzyme), is located in the inner mitochondrial membrane of the adrenal cortex and the other steroidogenic tissues.<sup>58</sup> CYP11A1 converts cholesterol to pregnenolone, precursor for all steroid hormones, that represents the first and also rate-limiting step of the biosynthesis of steroid hormones.<sup>59-61</sup>

Even though CYP11A1 is membrane attached, it lacks the N-terminal transmembrane anchor as is typical for microsomal CYPs. <sup>62</sup> CYP11A1-membrane interaction is represented by membrane-faced amino acids on the distal side of the enzyme mainly by F/G loop. <sup>63,64</sup> This was also confirmed by cysteine side chain mutagenesis studies in combination with fluorescent labelling of mutated residues suggested association of F/G loop of 11A1 with phospholipid vesicles. <sup>65</sup> Replacements of N210S/V211M and L218R/F219Y in putative F/G loop of *E. Coli* CYP11A1 lead almost to 2-fold increase of the turnover i.e. increase of P450 presence in the cytosol after protein expression. <sup>64</sup> A' helix and F/G loop were also identified as a membrane contact region deduced from hydrophobicity profiles of CYP11A1. Moreover, deletion within putative A helix caused protein expression instabilities indicating importance of this region on membrane binding. <sup>65</sup> Although the absence of the transmembrane anchor is the main distinguishing feature between microsomal and mitochondrial CYPs, the character of the interaction with membrane lipids thus remains similar.

The composition of lipid bilayers significantly affects the behavior of membrane attached CYPs, as well as their catalytic activities. It has been shown that the presence of overall neutral phosphatidylcholine and phosphatidylethanolamine lipids increased the catalytic activity of CYP2B4.<sup>66</sup> In addition, the presence of negatively charged phosphatidic acid (PA) and phosphatidylserine increased catalytic activity by 2-3-fold and 6-fold for CYP1A2 and CYP3A4 respectively.<sup>67,68</sup> The mitochondrial membranes are heterogeneous systems composed of both neutral and anionic lipids components roughly in ratio PC:PE:cardiolipin 2:2:1.<sup>69</sup>

The presence of cardiolipin in mitochondrial membranes significantly alters CYP11A1 behavior. According to the rotational diffusion experiments mobility of the protein depends on the cardiolipin concentration.<sup>70</sup> Cardiolipin has significant effect to the anchoring and embedding of CYP11A1 to the membrane bilayer caused probably by specific interaction with the negatively charged cardiolipin headgroups.<sup>70</sup> Moreover, the presence of phosphatidylcholines with branched fatty acyl chains elevates the activity of CYP11A1 and enhances the cholesterol binding.<sup>71</sup>

In this work, we studied the behavior of mitochondrial CYP11A1 on mitochondrial membrane model (POPC:POPE:cardiolipin in 2:2:1 molar ratio) in comparison to simple pure DOPC bilayer that was previously used as simplified membrane model for microsomal membranes.<sup>29,62</sup> We focused on the atomistic description of interactions of protein with individual lipids as well as on protein immersion, mutual membrane-protein orientation and their contact regions. We observed significant differences in terms of immersion and orientation of CYP11A1 in comparison to microsomal CYPs that is also reflected by the selection of the redox partners.

### 5.4.1 Behavior of CYP11A1 on DOPC

Up to this date both experimental and theoretical studies rationalized the role of lipid bilayer on mutual CYPs-membrane interaction, orientation, and the ability of CYPs to uptake drugs and release of its metabolites via the network of access and egress channels mainly on simple membrane models such as single component liquid disordered DOPC lipid bilayer as a baseline for membrane-protein interactions. As was shown previously for example in our studies of CYP3A4 on the membrane with various ratios of cholesterol<sup>72</sup> or on membranes containing lipids with different head groups<sup>73</sup>, the membrane composition is, however, important for overall behavior of membrane-attached CYP proteins.

To investigate the behavior of CYP11A1 on DOPC membrane, three separate MD simulations of 500 ns each were carried out. The structural fold of CYP11A1 was preserved with the root mean square deviation (RMSD) not exceeding 0.4 nm with respect to original crystal structure. Despite the conservation of protein secondary structure, the CYP11A1-DOPC membrane interaction changed significantly over time. The number of hydrogen bonds between protein and DOPC membrane decreased to the half from original pose from 34 counts to an average of  $\sim$ 16 hydrogen bonds depicting a weak interaction with protein surface (Figure 19 panel A). Moreover, the HTA showed significant differences between individual 500-ns long replica MD simulations (Figure 19 panel B). The individual three replicas with averaged HTA at 76.0  $\pm$  8.7 deg,  $57.0 \pm$  8.8 deg and  $62.2 \pm$  7.7 deg.

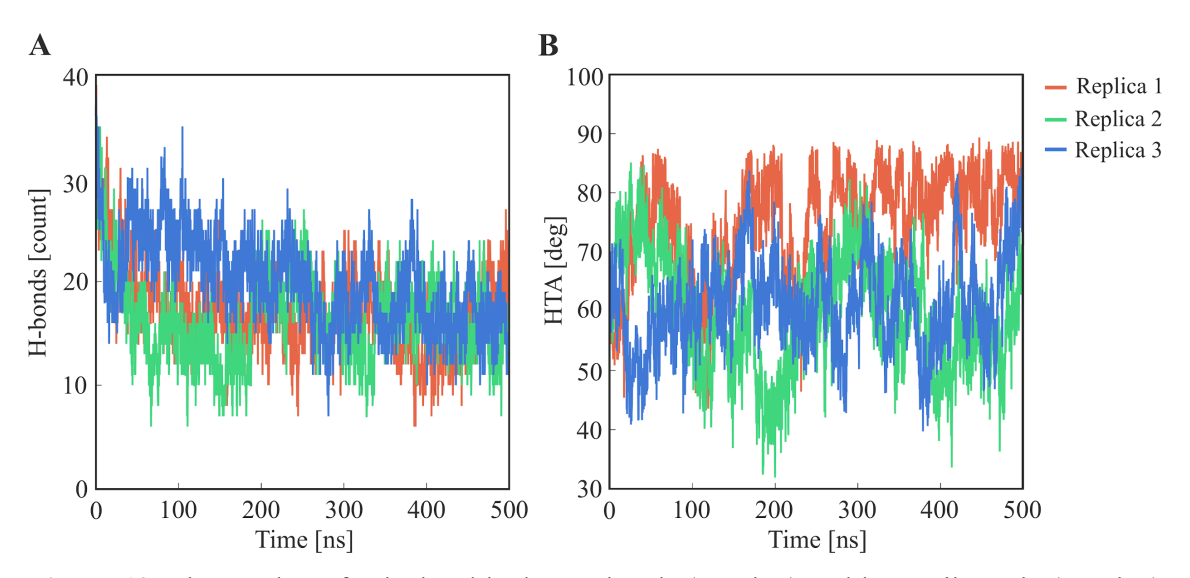


**Figure 19.** The number of calculated hydrogen bonds (panel A) and heme tilt angle (panel B) over the course of 500 ns simulation for three separate replicas. The diminishing of CYP11A1-DOPC membrane interactions is portrayed by the decrease of calculated hydrogen bonds between CYP11A1 and DOPC membrane and changes of HTAs.

Weak mutual CYP11A1 DOPC membrane interactions resulted in completely dissimilar final structures and different interactional patterns between individual replicas (Figure 20). Such behavior is quite dissimilar to the common structure of CYP3A4 or other microsomal CYPs which show strong and experimentally measurable unique HTA.<sup>29,74</sup>

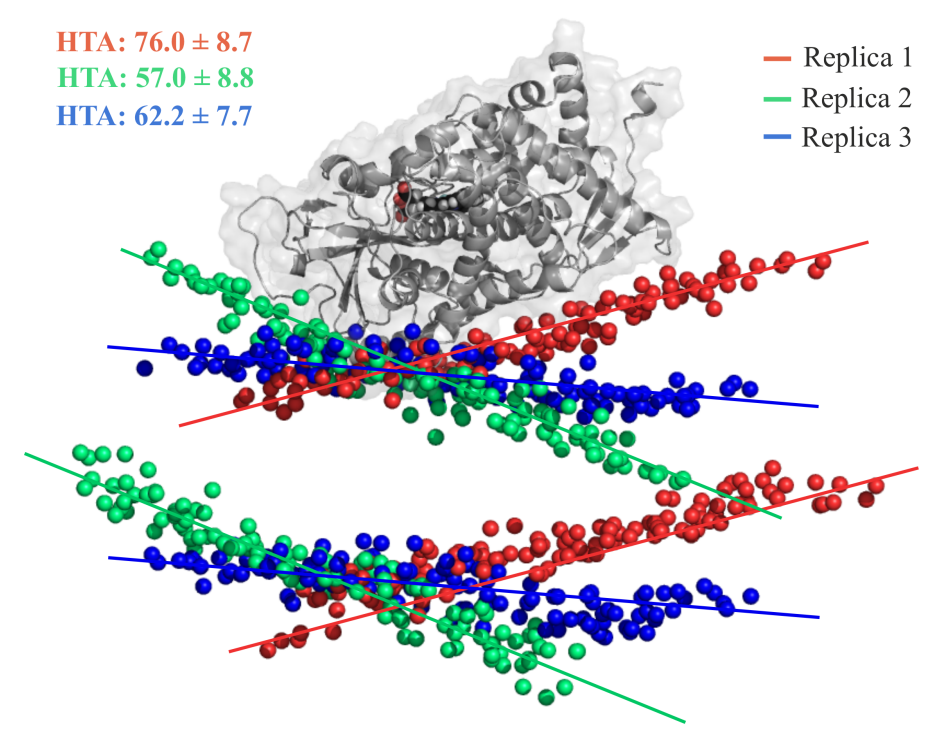


**Figure 20.** Snapshots of final structures from three separate replicas aligned by the catalytic sites of CYP11A1. Each replica shows significant changes in calculated HTAs. The loss of most CYP11A1-membrane interactions leads to completely different orientations of protein on DOPC membrane surface. CYP11A1 represented as cartoon with transparent surface. Phosphate atoms of DOPC headgroups depicting membrane surface showed as spheres.

### 5.4.2. Interaction of CYP11A1 with mitochondrial membrane

The composition of lipid bilayers significantly affects the behavior and stability of membrane-integrated proteins. The simple DOPC lipid though widely acknowledged and used in as membrane model, showed great instability in case of CY11A1 simulations. Those discrepancies manifested in unstable CYP11A1-DOPC interactions, orientation and tilt may be caused by the lack of electrostatic interactions governing the process of protein-membrane binding. Following those findings, we employed simulation of CYP11A1 of membrane mimicking the composition of inner mitochondrial (MIT) membrane. Three replica of systems containing CYP11A1 embedded into mitochondrial mimicking memebrne (POPC:POPE:cardiolipin in 2:2:1 molar ratio) were simulated for total of 500 ns production run in order to investigate protein stability and protein-membrane interactions. CYP11A1 was stable during three 500 ns-long MD simulations with the RMSD not exceeding 0.4 nm (with respect to crystal structure) converging into the same CYP11A1-MIT orientations and tilt. Moreover, the CYP11A1-MIT interaction pattern corresponds closely to previously obtained results from both, theoretical models and experimental measurements.

The initial interaction of the CYPs with MIT membrane followed the general contact region localized on the distal side of the enzyme. During the first ~40 ns of 500 ns simulations the mutual protein-membrane orientation shifted leaving the distance of catalytic domain of CYP11A1 and MIT membrane at ~4.5 nm from original value of 3.9 nm. This led to omitting most interactions from its original pose and change of the tilt of the protein to (HTA of 22.11-26.43 deg with respect to individual replicas) on membrane surface adopting more vertical orientation of CYP11A1.

While the soluble protein did not keep its original immersion within the membrane core the interaction remained stable during the whole production run. The tight association is important for CYP11A1 uptake of water insoluble cholesterol molecules from hydrophobic membrane environment via the net of access channels. Analysis of minimal distances between CYP11A1 and MIT membrane showed interaction patterns on distal side of namely on A' helix, F/G loop, and part of protein secondary structure motifs corresponding to G helix, B'helix, β1 sheet and β2 sheet (Figure 21). The tightest membrane association was observed for A' helix and F/G loop. It was previously shown that deletion of A' helix decreases the amount of expressed CYP11A1 protein association with bacterial *E. coli* membrane. Previous theoretical model also pointed out hydrophobic patches involving tryptophan residues in F/G loop region as potential membrane binding domain. Moreover, the enhance of fluorescence signal for cysteine mutants in this region showed the association of F/G loop and most likely of C-terminal part of G helix with lipid

vesicles.<sup>65</sup> Side chain mutations of F/G loop also affects the subcellular distribution of enzyme associated with bacterial membrane.<sup>64</sup> The terminal part of G helix following the F/G loop segment was also in close contact with MIT membrane in our models (Figure 21).

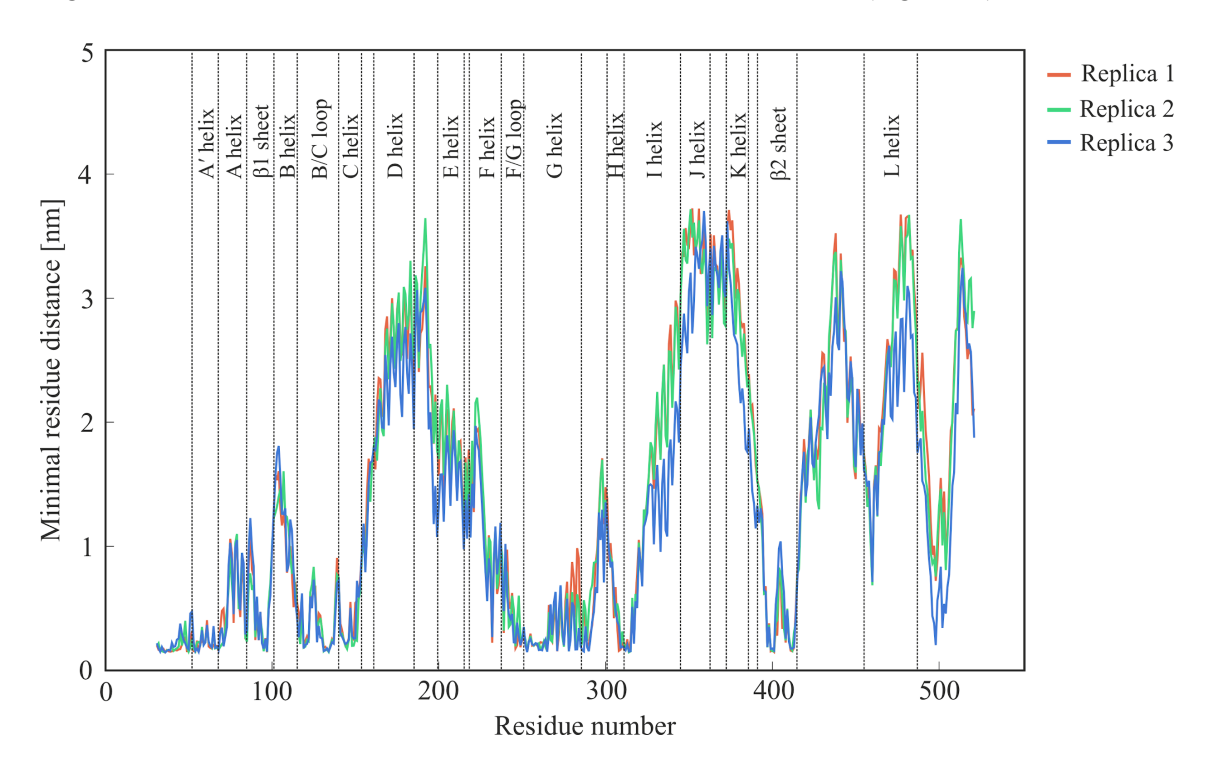


**Figure 21.** Minimal distances of individual amino acid CYP11A1 residues from MIT membrane. Secondary structure motifs of CYP11A1 depicted in the upper panel. Interaction with MIT membrane can be seen via A' helix, B/C loop, C helix, F/G loop, G helix and  $\beta$ 2 sheet.

**Table 2.** Measured averages and standard deviations for CYP11A/MIT simulations in 3 replicas.

CYP11A10-MIT*	REP1	REP2	REP3
distance/height [nm]	$4.50\pm0.12$	$4.48 \pm 0.13$	$4.51 \pm 0.16$
num. of H-bonds [count]	$32.47 \pm 4.47$	$31.43 \pm 6.13$	$23.99 \pm 4.22$
HTA [deg]	$22.11 \pm 8.21$	$21.85 \pm 6.43$	$26.43\pm6.85$
A' helix [nm]	$2.42\pm0.20$	$2.33 \pm 0.16$	$2.57 \pm 0.19$
F/G loop [nm]	$2.31\pm0.14$	$2.40 \pm 0.14$	$2.43 \pm 0.12$
R90-Y100 (β1 sheet) [nm]	$2.71\pm0.14$	$2.46 \pm 0.12$	$2.81 \pm 0.14$
H130-G138 (B'helix) [nm]	$2.61 \pm 0.19$	$2.76 \pm 0.24$	$2.61 \pm 0.27$
T260-W270 (G helix) [nm]	$2.67 \pm 0.21$	$2.88 \pm 0.18$	$2.48 \pm 0.16$
L398-L402 (β2 sheet) [nm]	$2.75 \pm 0.19$	$2.70 \pm 0.19$	$3.00\pm0.17$
P410-V415 (β2 sheet) [nm]	$2.70\pm0.14$	$2.54 \pm 0.15$	$2.83 \pm 0.14$

<sup>\*</sup> distances measured as the COMs between CYP11A1 or individual protein segments and MIT membrane in z-axis

The composition of mixed lipid bilayer mimicking the inner mitochondrial membrane played crucial role on overall CYP11A1-membrane interaction pattern. Even though, the interaction of CYP11A1 and MIT membrane was omitted to the fraction of interactions from the initial immersed model (initial structure) their pattern was stable across all replicas (see above). The radial distribution function (Figure 22) of CYP11A1 surface with the center of masses of closest lipid headgroup atoms showed that all lipid components interact at approximately same distance with sharp overlapping peaks of distribution distances at ~0.4 nm. The predominant interaction was observed in case of zwitterionic POPE lipid. For POPC lipid the interaction was reduced to almost half of POPE interactions with the same amount of lipid molecules taking into calculation. The least significant interaction pattern was observed in case of cardiolipin with negligible peak at closest distribution distances.

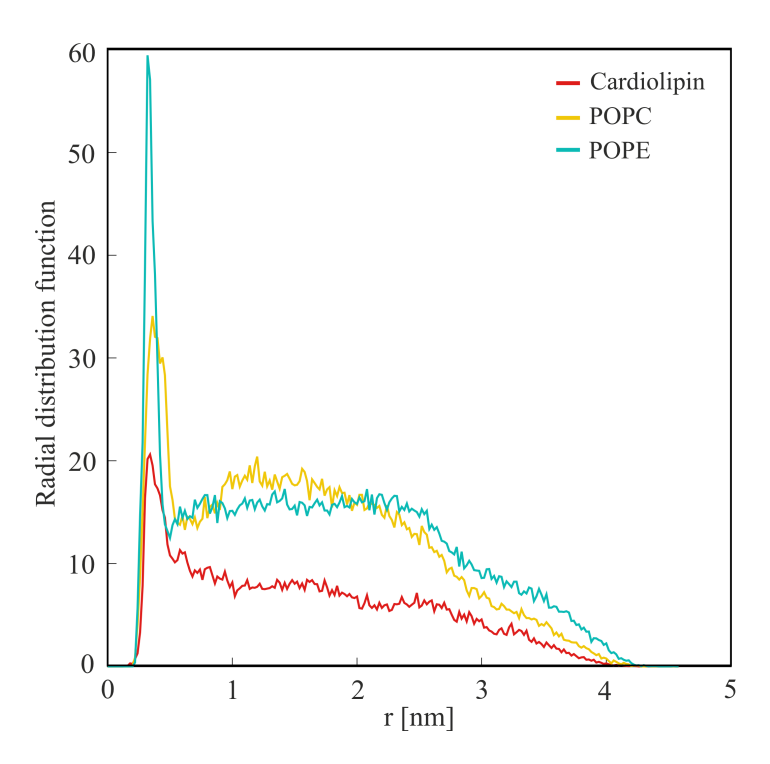


**Figure 22.** The radial distribution function measured between the surface of CYP11A1 and the center of masses of closest atoms in lipid headgroup in upper headgroup leaflet.

Even though the RDF showed less favorable interaction pattern for cardiolipin the presence of this highly negatively charged molecule was previously found crucial for mitochondrial CYP-membrane interaction. More detail analysis of CYP11A1-cardiolipin interaction revealed significant amount positively charged amino acids on CYP1A1 surface to be directly interacting or in close contact with anionic cardiolipin molecules. In total, 13 positively charged amino acids (8 arginines - R31, R43, R46, R67, R90, R135, R256 and R259; 5 lysines - K92, K143, K261, K264 and K412) located at proximity to cardiolipin headgroup surface (Figure 23). From those amino acids, arginines - R67 is locate in A' helix, R256 and R259 in F/G loop; lysines K261 and

K264 in G helix matching segments of CYP11A1 previously reported to interact with membrane. This may conclude, that even though the overall anchorless CYP11A1-MIT membrane interactions are looser in comparison to membrane-anchored CYPs, those electrostatically driven interaction may contribute to overall stability and preferable orientation of CYP11A1 on inner mitochondrial membrane.

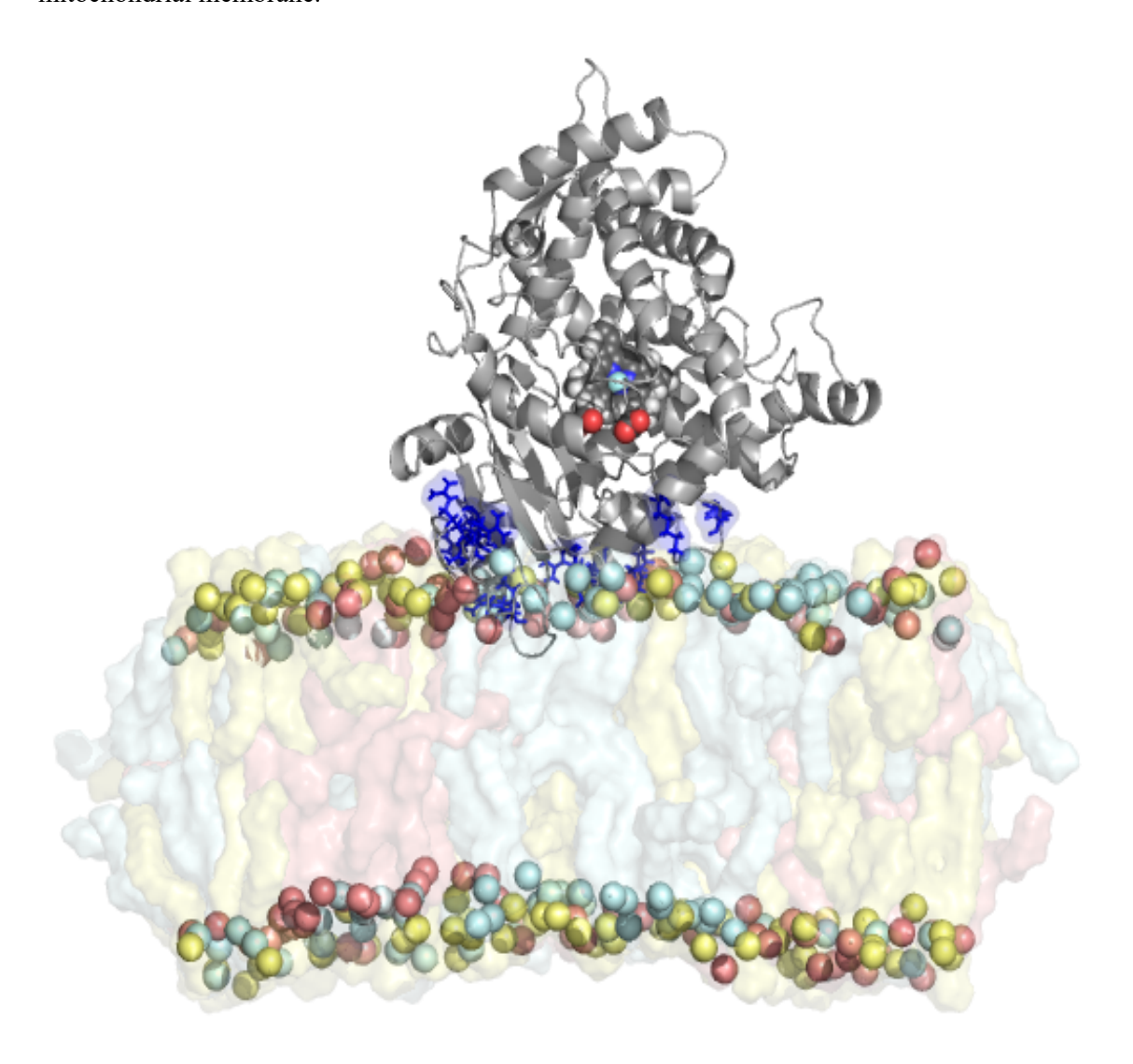


**Figure 23.** Final snapshot (500 ns) of CYP11A1 on mitochondrial membrane. Positively charged amino acids (presented as blue sticks) in close contact with cardiolipin headgroups showed as sticks. Phosphate atoms shown as spheres with rest of membrane in transparent representation (POPE in cyan, POPC in yellow, cardiolipin in pale red).

### 5.4.3. CYP11A1 channels dynamics

The active pocket of CYP11A1 is buried within the enzyme structure in the close proximity to the heme-binding region where the substrate - cholesterol - is metabolized. The CYP11A1 uptake of water-insoluble molecules (such as cholesterol) from the hydrophobic membrane environment is mediated via the net of access channels. Here, we characterized potential channels and their position and opening/closing during a 500-ns long simulation.

During the 500-ns long simulation, 5 main channels – S, 2e, 2a/x, 2e, 3 – were detected connecting the heme-binding cavity with the protein surface allowing the substrate/metabolite entrance/excess (Figure 24). Those channels are located on distal side of CYP11A1. One channel was recognized as channel solvent channel (S) egress from the heme-binding region and passes between E, F and I helices and  $\beta$ 3-4 sheets. Moreover, two channels from channels 2 subclass characterized as 2e passing through B/C loop and channel 2b egressing between B and B' helices and  $\beta$ 1 sheet. One additional channel, here denoted as channel 2ax, that was not described before and bears the most similarities to 2a channel. Channels 2b and 2e end within the membrane while the channels 2, 3, S or 2ax end above the membrane. Given that the CYP11A1 transforms cholesterol to slightly more polar pregnenolone, it can be hypothesized that cholesterol enters the CYP11A1 via channel 2e or 2b, while pregnenolone egress through channel S, 3 or channel 2ax.

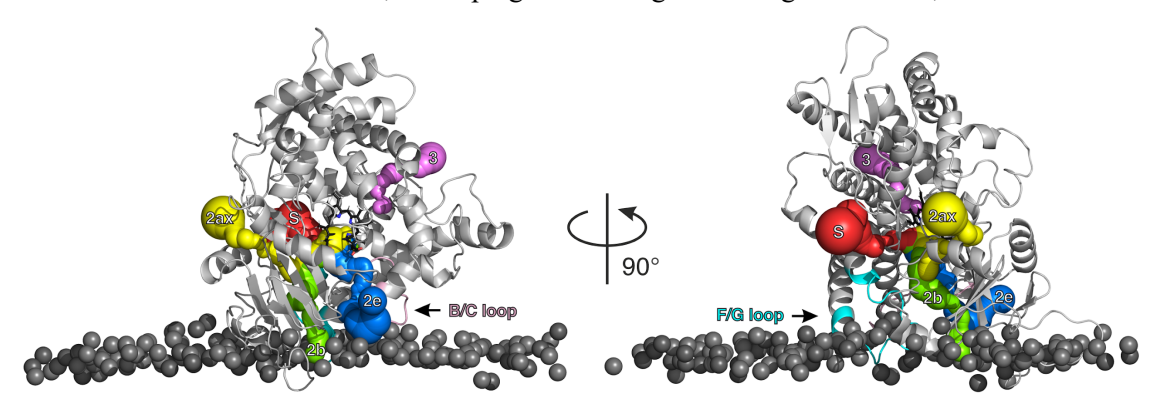


**Figure 24.** Characterization of access/egress channels of CYP11A1 on mitochondrial membrane. Left panel show final snapshot of CYP11A1 structure from proximal side of heme while the later one shows the side view rotated by 90° of the same structure. The phosphate atoms of lipid headgroups of upper lipid bilayer are shown as grey spheres. The access/egress channels radius is visualized by their radius. The channels here are characterized by standard nomenclature by Cojocaru et al. <sup>76</sup> and show as channel S (red), channel 2b (green), channel 2e (blue), channel 2ax (yellow) and channel 3 (violet).

#### 5.4.4. Interaction of CYP11A1 with Adrenodoxin

CYP11A1 is essential for synthesis of various steroid hormones such as cholesterol, where it catalyzes the cholesterol side-chain cleavage to pregnenolone. Prior to the biotransformation reactions the supply of electrons from its redox partner is needed. The primary electron carrier for mitochondrial CYP11A1 is adrenodoxin (Adx), which mediates electron transfer between adrenodoxin reductase (AdR) and CYP11A1 itself. In order to successfully mediate the electrons, the direct contact between Adx and CYP11A1 needs to occur resulting in stable Adx-CYP11A1 complex. Therefore, the appropriate mutual orientation of both redox partner is crucial. Here we rationalize the possible intra-protein interaction scenario based on our simulation of CYP11A1 on lipid bilayer mimicking the inner mitochondrial membrane where the second part of electron transfer chain takes place.

As shown above, the loose yet preserved interaction of CYP11A1-MIT membrane with monotopic orientation above membrane surface resulted in more vertical orientation of CYP11A1. This orientation exposes to water the proximal side of CYP11A1 where the binding of redox partner occurs. As reported previously, the interaction is driven by strong electrostatic attraction between negatively charged amino acid residues of Adx and positively charged CYP11A1 surface near heme containing region. Those basic residues located of protein surface are conserved among all mitochondrial CYP family. Since Adx is cleaved from terminal part of transit peptide it might approach its redox partner directly from mitochondrial matrix or from site of inner mitochondrial membrane to which it is loosely bound. Our model shows that either of those is scenarios is possible since the loose membrane association allows the CYP11A1 to orient its proximal face to approaching partner. Moreover, the K helix with conserved positive amino acid residues (K378, K382 and R386) facing the space above MIT membrane allows approach of Adx. Furthermore, C- and L- helices as well as the heme binding loop, previously reported as potential interaction regions, are also sterically oriented for potential intra-protein binding.

# 5.5 Membrane-attached Model of Cytochrome P450 Reductase: Simulations of naturally occurring states and of the complex by cytochrome P450 3A4

The biotransformation processes catalyzed by all mammalian CYPs depends on a supply of electrons from various of redox partners. In the microsomal electron transfer cascade redox equivalents are provided by cytochrome P540 reductase (CPR) and cytochrome b<sub>5</sub>. In microsomes, proteins involved in electron transport chain are membrane-attached proteins located on the cytosolic side of the endoplasmic reticulum.

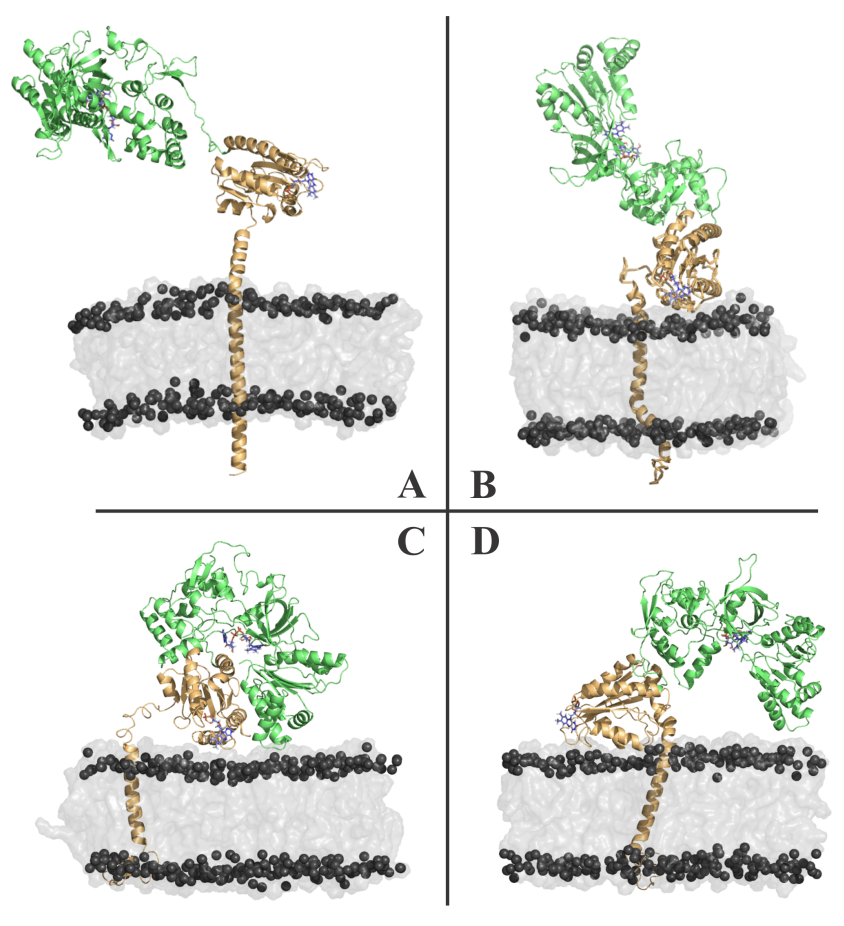
This chapter summarizes a comprehensive study of membrane-attached CPR in various biologically relevant states. We conducted molecular dynamics simulations of CPR in both closed and open conformations investigating the stability of both conformations and its interactions with membrane model composed of DOPC. Furthermore, we conducted metadynamics simulations revealing the mechanism of CPR transition from open to closed state. Resulting models further served as a necessary step to establish fully atomistic model of stable CYP-CPR complex on membrane depicting mutual interaction sides of microsomal redox partners.

### 5.5.1 Models of CPR in closed and open conformations

Model of membrane-attached CPR in closed conformation was very stable during 700 ns simulations. There were no structural changes suggesting spontaneous transition into open conformation. Orientation of CPR domains remained unchanged leaving them (as well as all containing cofactors) in direct contact necessary for intra-protein electron transfer. Also hinge region, often found to be responsible for structural changes between open and closed form, showed no significant changes which could lead to conformation transformation. We measured the height of globular part of CPR above the membrane as  $5.6 \pm 0.4$  nm which is in a great agreement with experimental value of  $5.6 \pm 2.2$  nm provided by AFM measurement.<sup>77</sup>

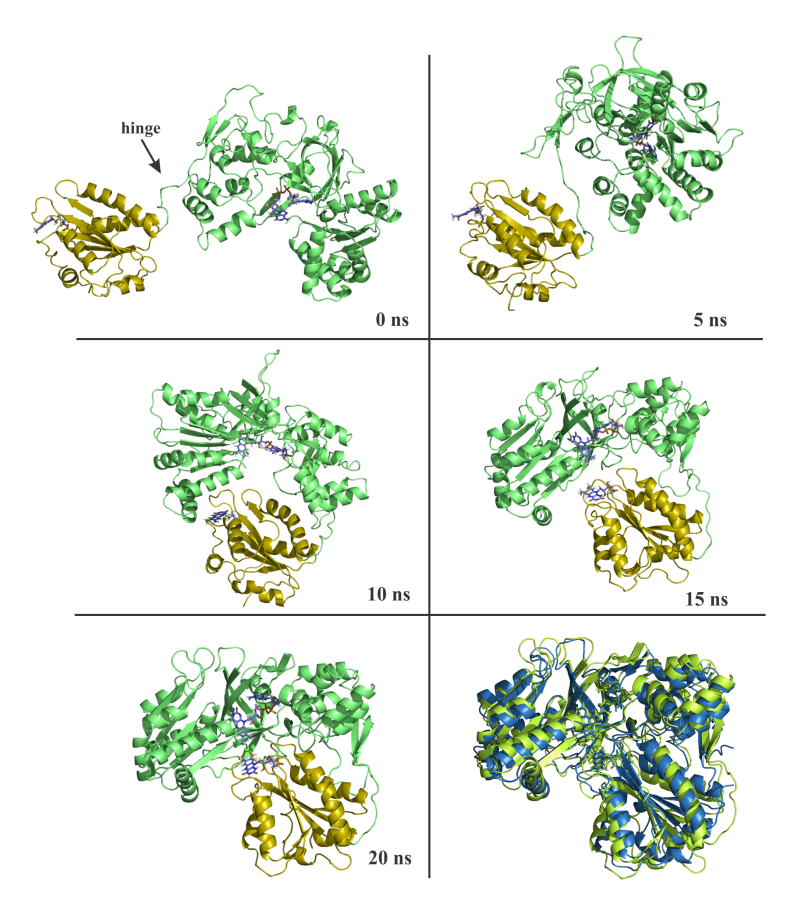
We also investigated our model in terms of interaction amino acid residues of catalytic domain which are in contact with DOPC membrane. We identified those residues E270-P275, I307-R313 and N464 from the FAD domain, W549-G554 in NADPH binding domain as point of contacts with the membrane. Those interactions stabilized the position of CPR on membrane and restricted additional free reorientation of protein upon membrane surface.

In contrast to stable and compact closed conformation, in an open crystal conformation, both domains are in great distance from each other leaving flavin cofactors 86 Å apart. In this condition CPR binds CYP and reduces its iron atom in heme since the FMN binding domain is exposed and the FMN cofactor is reveled enabling the possible interaction to its redox partners. As our model shows, CPR in open conformation is in principle able to interact with its redox partner (e.g., the favorable orientation and FMN cofactor exposure) but it is not (as opposite to closed CPR) supported by contact with membrane and the mobility of catalytic domains is therefore unrestricted. Moreover, FAD, linker and NADPH binding domains are connected freely with FMN domain via hinge region and are exposed to the solvent environment. Three independent replica simulations revealed instability of opened form resulting into different scenarios (Figure 25). Resulted structures deviated greatly from its crystal structure mostly with the most noticeable difference in mutual orientations of flavine domains especially at hinge region. While the internal structures of each catalytic domain remained intact, mutual mobility of catalytic domains was observed. In all simulations, however, the FMN domain is turned toward membrane inaccessible for interaction with redox partner.



**Figure 25.** Snapshots of open structures of CPR in different conditions. Panel A represents starting structure for simulations of CPR in open conformation embedded in DOPC bilayer. Panels B, C and D represent different structural changes after 100 ns simulations. In all three scenarios FMN domains are in direct contact with membrane surface disallowing electron transfer to CYPs to occur.

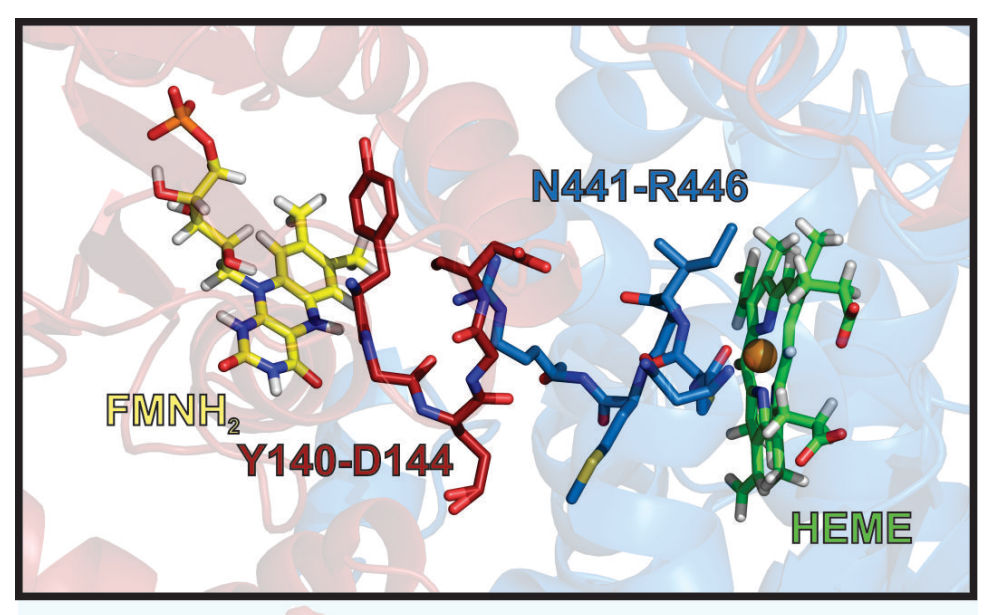
Because no spontaneous closing was observed during classical MD simulations of CPR in open conformation additional metadynamics simulations were employed. An external bias potential was applied on distance root mean square deviation (DRMSD) of protein backbone of amino acid residues F201-V345 (including the hinge region) as collective variable during conformation transition from open to closed conformation. During ~20 ns MTD simulation protein adopted compact conformation comparable with crystal structure of CPR in closed conformation. The process of conformation transition can be described as following. At first, mutual reorientation between FMN domain and the rest of catalytic domain occurred (Figure 26 at time of 5 ns). The rotation movement was conducted by flexible hinge region. Then catalytic domains approached closer. FAD, linker and NADPH domains are approaching FMN domain from (Figure 26 at times of 10 and 15 ns) its upper part where helixes A183-L192 and E213 and E229 are located. At last, the front part of FMN domain, where FMN cofactor molecule is located was covered by the rest of catalytic domain leaving flavin cofactors at distance of ~5 Å in positions corresponding with crystal structure of closed CPR (Figure 26 at time of 20 ns). After complete closure, CPR was inappropriately oriented on membrane surface resulting in no successive opening.



**Figure 26.** Conformation changes of CPR from open to closed conformation. that occurred during 20 ns of metadynamics simulations. After 20 ns, protein adopts as well as cofactors adopted structure identical with crystal structure of CPR in closed conformation. The last images represent aligned structures after 20 ns of MTD simulation (green) with crystal structure of CPR (blue). Protein shown in cartoon representation (FMN domain gold; the rest of catalytic domains green) with cofactors as sticks (blue).

### 5.5.2 Model of membrane-attached CPR-CYP 3A4 complex

Since the main role of cytochrome P450 reductase is electron supply to its redox partners from cytochrome P450 family, we studied model of inter-protein complex of CPR and cytochrome P450 3A4, both embedded in membrane. The model was created using CPR in open conformation as an electron donor protein. In the starting position, proteins were oriented, so CYP faced with proximal site of heme molecule to exposed FMN cofactor. In course of 400 ns simulation FMNH<sub>2</sub> - heme molecule distance dropped from original value of 29.6 Å to constant value of  $21.7 \pm 0.5$  Å (at the closest approach at 18.3 Å) resulting in a very stable protein complex in contrast with open CPR conformation itself. Strong interaction between those redox partners was mainly driven by electrostatic forces due to oppositely charged amino acid residues at interaction sites of proteins. Strong interaction of proteins as well as sufficient distance between cofactors made our purposed model valid for study of possible protein-protein interaction and electron transfer pathways. In CPR-CYP3A4 complex (Figure 27), nitrogen N5 atom of FMNH2 molecule is oriented towards heme cofactor molecule allowing electron transfer to occur. On redox partners, loops that may be important for electron transport were defined as Y140-D144 (Y140, G141, E142, G143 and D144) in CPR structure and Asn441-Arg446 (N441, C442, I443, G444, M445, R446) in CYP3A4 structure. Those residues are located directly between FMNH<sub>2</sub> and heme cofactors at the side of interaction. Amino acid residues of C442, M445 and R446 of CYP 3A4 were previously proposed to be involved in interaction with redox partners.<sup>78</sup> Moreover, side chain mutation R446A of CYP 2B4, located at same region as R446 at CYP 3A4, lead to decrease of interaction with CPR.<sup>79</sup> In addition, recent solution NMR study clarified interaction sites of CPR with redox partners, namely cytochrome P450 17A1 as Loop 1 of CPR (87QTGT<sup>90</sup>).80 Our model of membrane bound CYP-CPR complex meets those experimental data for binding site of CPR as the Loop 1 located at close proximity to FMNH<sub>2</sub> cofactor was found in direct contact with CYP 3A4 in our simulation.



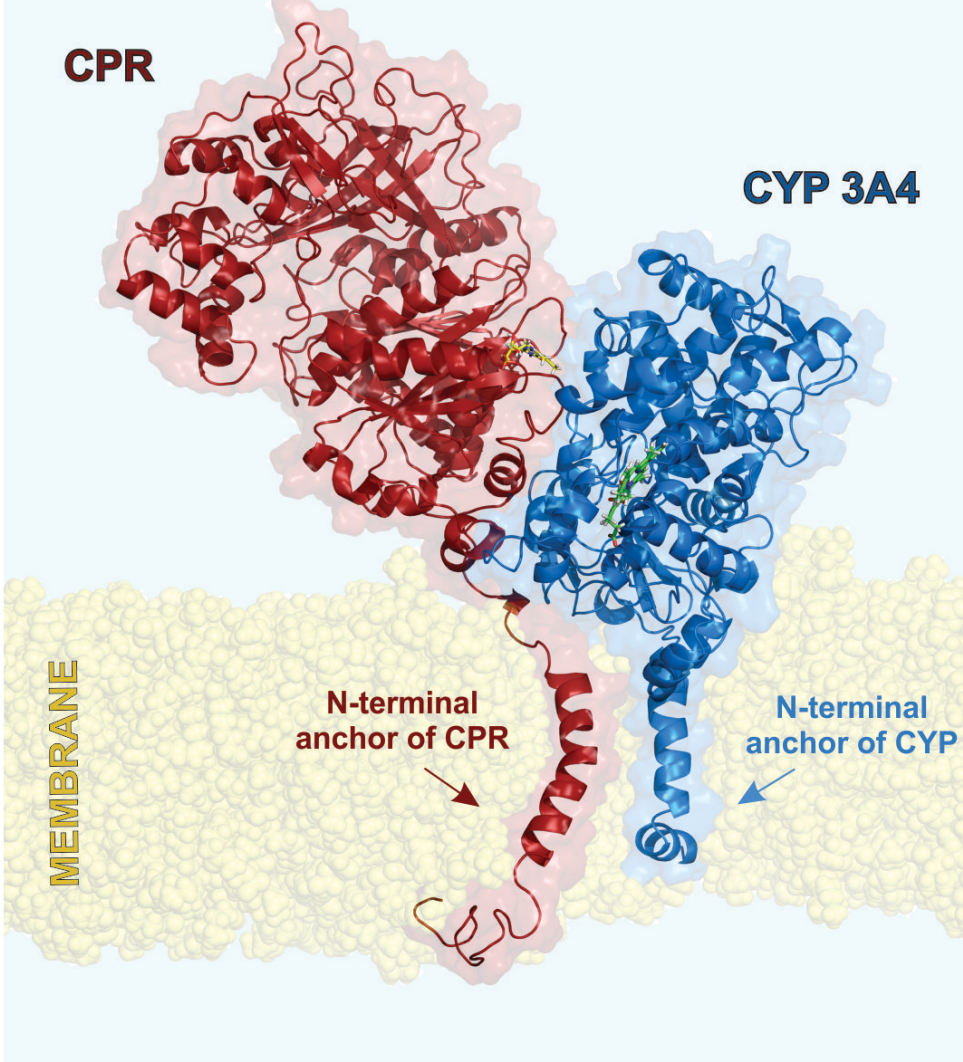


**Figure 27.** Final structure of human CPR-CYP3A4 complex embedded in DOPC membrane. The FMNH $_2$  and heme cofactors were located at proximity with residues including the Y140-D144 loop of CPR and N441-R446 of CYP3A4 as possible electron transfer mediators.

### 6. Summary

This dissertation thesis focuses on exploring the significance of biological membranes through a range of computational techniques, encompassing the utilization of scientific databases, precise quantum mechanical calculations, and investigating their dynamic behaviour using molecular dynamics simulations.

Initially, our focus was on the development of a scientific database aimed at curating and rationalizing the interactions between molecules and membranes. These interactions play a crucial role in the actions of individual molecules within an organism, as well as in their pharmacokinetics and pharmacodynamics. However, currently, these valuable data are not interconnected and are scattered across various platforms and literature sources, resulting in a lack of comprehensive benchmark comparisons among different experimental and theoretical methods for studying membrane systems. To address this issue, we created the Molecules on Membrane database (MolMeDB). Here, I present the process of developing and utilizing this database, along with highlighting its significant advantages. These advantages include facilitating direct comparisons of results from various entries, showcasing examples of membrane interactions involving caffeine and its metabolites, as well as enabling the comparison of large datasets obtained from different theoretical methods.

Subsequently, our focus shifted towards investigating the permeation of cyclosporin A, a widely used immunosuppressant, across various models of biological membranes. Through enhanced molecular dynamics (MD) simulations, we discovered that the composition of the membrane significantly influences the mechanism of CsA permeation. In simplified phosphatidylcholine membrane models, the energetical profiles for CsA passage were relatively similar. However, the presence of cholesterol induced changes in the membrane's ordering, leading to a shift of the energetical minima directly towards the centre of the lipid bilayer when equimolar concentrations of cholesterol and phosphatidylcholine were present. The borderline case of DPPC also revealed that CsA was unable to permeate through membranes in the gel-ordered phase. In all cases, the strongly hydrophobic nature of CsA and its limited water solubility indicated that CsA primarily resides within the aliphatic interior of the membrane. These findings shed light on the importance of membrane composition on the permeation of CsA and highlight the preferential localization of CsA within the lipid bilayer.

Then, our research focused on the development and validation of a systematic computational methodology for predicting suitable liposomal encapsulation and thermally induced release of bio-active compounds. By combining classical molecular dynamics (MD) simulations with

quantum chemistry-based calculations, we were able to establish selection criteria for identifying compounds capable of stable encapsulation and temperature-induced release from liposomes. To explore a wide range of potential candidates, we performed an *in silico* screening of the DrugBank database against these selection criteria. This analysis led us to identify a new drug, cycloserine, as a promising candidate for tailored liposomal loading and thermal release. Through our computational/experimental approach, we have paved the way for more efficient and targeted encapsulation and release of bio-active compounds using liposomes. Our methodology allows *in silico* design and optimization of liposomal drug delivery systems.

In a subsequent study on the effect of membrane composition role, our aim was to elucidate the influence of membrane lipid composition on the behaviour of mitochondrial cytochrome P450 CYP11A1 enzyme. To achieve this, we investigated the enzyme's behaviour on two distinct membrane models: a simple DOPC bilayer and a more complex membrane mixture with cardiolipin mimicking mitochondrial lipid composition. Our findings revealed that using a simple pure DOPC membrane model inadequately captures the interactions between the membrane and CYP11A1 enzyme. Specifically, the simulation results showed different interaction patterns when employing a multiple-replica simulation setup. In contrast, employing a more complex model mimicking the composition of the mitochondrial membrane more accurately described the mutual orientation and immersion of CYP11A1 in relation to experimental data. Our investigation concluded that while the overall interactions between anchorless CYP11A1 and the mitochondrial membrane are less tight compared to membrane-anchored CYPs, these interactions, which are primarily driven by electrostatic forces, may contribute to the overall stability and preferred orientation of CYP11A1 on the inner mitochondrial membrane. These findings shed light on the intricate interplay between membrane lipid composition and the behaviour of CYP11A1.

The final project of this thesis focuses on studying the behaviour of membrane-attached cytochrome P450 reductase (CPR) and its interactions with its redox partner, cytochrome P450 CYP3A4. Our investigation revealed that in the closed conformation, CPR adopts a highly compact structure reminiscent of its crystal form. This structural stability is facilitated by its close association with the membrane. On the other hand, when bound in a DOPC membrane model, the open form of CPR was found to be unstable, and the resulting structures were unable to interact effectively with its redox partner CYP3A4. However, we observed significant mutual stabilization between the interacting CPR and CYP3A4 proteins. Through this model, we identified several amino acids located in the proximal site of CYP3A4 and the FMN binding site of CPR that are involved in protein-protein electron transport. These findings provide valuable insights into the dynamic behaviour and interplay between CPR and CYP3A4 in a membrane context.

### 7. References

- 1. Harayama, T. & Riezman, H. Understanding the diversity of membrane lipid composition. *Nat. Rev. Mol. Cell Biol.* **19**, 281–296 (2018).
- 2. Fong, T. M. & Mcnamee, M. G. Stabilization of Acetylcholine Receptor Secondary Structure by Cholesterol and Negatively Charged Phospholipids in Membranes. *Biochemistry* **26**, 3871–3880 (1987).
- 3. Braverman, N. E. & Moser, A. B. Functions of plasmalogen lipids in health and disease. *Biochim. Biophys. Acta Mol. Basis Dis.* **1822**, 1442–1452 (2012).
- 4. Koynova, R. & Caffrey, M. Phases and phase transitions of the phosphatidylcholines. *Biochim. Biophys. Acta Rev. Biomembr.* **1376**, 91–145 (1998).
- 5. Dufourc, E. J. Sterols and membrane dynamics. *J. Chem. Biol.* 1, 63–77 (2008).
- 6. van Meer, G., Voelker, D. R. & Feigenson, G. W. Membrane lipids: where they are and how they behave. *Nat. Rev. Mol. Cell Biol.* **9**, 112–124 (2008).
- 7. Casares, D., Escribá, P. V. & Rosselló, C. A. Membrane lipid composition: Effect on membrane and organelle structure, function and compartmentalization and therapeutic avenues. *Int. J. Mol. Sci.* **20**, 1–30 (2019).
- 8. Yang, N. J. & Hinner, M. J. Getting Across the Cell Membrane: An Overview for Small Molecules, Peptides, and Proteins. *Methods Mol. Biol.* **1266**, 29–53 (2015).
- 9. Walter, A. & Gutknecht, J. Permeability of small nonelectrolytes through lipid bilayer membranes. *J. Membr. Biol.* **90**, 207–217 (1986).
- 10. Cossart, P. & Helenius, A. Endocytosis of Viruses and Bacteria. *Cold Spring Harb. Perspect. Biol.* **6**, a016972–a016972 (2014).
- 11. Lipinski, C. A., Lombardo, F., Dominy, B. W. & Feeney, P. J. Experimental and computational approaches to estimate solubility and permeability in drug discovery and development settings. *Adv. Drug Deliv. Rev.* **46**, 3–26 (2001).
- 12. Palm, K., Stenberg, P., Luthman, K. & Artursson, P. Polar molecular surface properties predict the intestinal absorption of drugs in humans. *Pharmaceutical Research* vol. 14 568–571 (1997).
- 13. Rezai, T., Yu, B., Millhauser, G. L., Jacobson, M. P. & Lokey, R. S. Testing the conformational hypothesis of passive membrane permeability using synthetic cyclic peptide diastereomers. *J. Am. Chem. Soc.* **128**, 2510–2511 (2006).
- 14. White, T. R. *et al.* On-resin N-methylation of cyclic peptides for discovery of orally bioavailable scaffolds. *Nat. Chem. Biol.* 7, 810–817 (2011).
- 15. Potts, R. O. & Guy, R. H. Predicting Skin Permeability. *Pharm. Res. An Off. J. Am. Assoc. Pharm. Sci.* **9**, 663–669 (1992).
- 16. Jalili, S. & Saeedi, M. Study of curcumin behavior in two different lipid bilayer models of liposomal curcumin using molecular dynamics simulation. *J. Biomol. Struct. Dyn.* **34**, 327–340 (2016).
- 17. Qiao, B. & de la Cruz, M. O. Driving Force for Water Permeation Across Lipid Membranes. *J. Phys. Chem. Lett.* **4**, 3233–3237 (2013).
- 18. Paloncýová, M., Berka, K. & Otyepka, M. Molecular insight into affinities of drugs and their metabolites to lipid bilayers. *J. Phys. Chem. B* **117**, 2403–2410 (2013).
- 19. Mathai, J. C., Tristram-Nagle, S., Nagle, J. F. & Zeidel, M. L. Structural determinants of water permeability through the lipid membrane. *J. Gen. Physiol.* **131**, 69–76 (2008).
- 20. Chapman, D. Penkett, S. A. Nuclear Magnetic Resonance Spectroscopic Studies of the Interaction of Phospholipids with Cholesterol. *Nature* **211**, 1304–1305 (1966).
- 21. Finkelstein, A. Cass, A. Effect of cholesterol on the water permeability of thin lipid membranes. *Nature* **216**, 717–718 (1967).
- 22. Papahadjopoulos, D. Nir, S. Oki, S. Permeability properties of phospholipid membranes: effect of cholesterol and temperature. *Biochim. Biophys. Acta* **226**, 561–583 (1972).
- 23. Eriksson, E. S. E. & Eriksson, L. A. The Influence of Cholesterol on the Properties and Permeability of Hypericin Derivatives in Lipid Membranes. *J. Chem. Theory Comput.* 7, 560–574 (2011).

- 24. Wennberg, C. L., van der Spoel, D. & Hub, J. S. Large influence of cholesterol on solute partitioning into lipid membranes. *J. Am. Chem. Soc.* **134**, 5351–5361 (2012).
- 25. Ottaviani, G., Martel, S. & Carrupt, P.-A. Parallel Artificial Membrane Permeability Assay: A New Membrane for the Fast Prediction of Passive Human Skin Permeability. *J. Med. Chem* **49**, 3948–3954 (2006).
- 26. Kansy, M., Senner, F. & Gubernator, K. Physicochemical High Throughput Screening: Parallel Artificial Membrane Permeation Assay in the Description of Passive Absorption Processes. *J. Med. Chem.* **41**, 1007–1010 (1998).
- 27. Hidalgo, I. J., Raub, T. J. & Borchardt, R. T. Characterization of the human colon carcinoma cell line (Caco-2) as a model system for intestinal epithelial permeability. *Gastroenterology* **96**, 736–49 (1989).
- 28. McDonell, A. M. & Dang, C. H. Basic Review of the Cytochrome P450 System. *J. Adv. Pract. Oncol.* **4**, 263–268 (2013).
- 29. Šrejber, M. *et al.* Membrane-attached mammalian cytochromes P450: An overview of the membrane's effects on structure, drug binding, and interactions with redox partners. *J. Inorg. Biochem.* **183**, 117–136 (2018).
- 30. Shephard, E. A., Phillips, I. R., Bayney, R. M., Pike, S. F. & Rabin, B. R. Quantification of NADPH: cytochrome P -450 reductase in liver microsomes by a specific radioimmunoassay technique. *Biochem. J.* **211**, 333–340 (1983).
- 31. Flück, C. E. *et al.* Mutant P450 oxidoreductase causes disordered steroidogenesis with and without Antley-Bixler syndrome. *Nat. Genet.* **36**, 228–230 (2004).
- 32. Shephard, E. A. *et al.* Isolation of a Human Cytochrome P-450 Reductase cDNA Clone and Localization of the Corresponding Gene to Chromosome 7q11.2. *Ann.Hum.Genet.* **53**, 291–301 (1989).
- 33. Difilippo, E. L. & Eganhouse, R. P. Assessment of PDMS-Water Partition Coefficients: Implications for Passive Environmental Sampling of Hydrophobic Organic Compounds. *Environ. Sci. Technol.* **44**, 6917–6925 (2010).
- 34. Endo, S., Escher, B. I. & Goss, K.-U. Capacities of membrane lipids to accumulate neutral organic chemicals. *Environ. Sci. Technol.* **45**, 5912–5921 (2011).
- 35. van Breemen, R. B. & Li, Y. Caco-2 cell permeability assays to measure drug absorption. *Expert Opin. Drug Metab. Toxicol.* **1**, 175–185 (2005).
- 36. Avdeef, A. *et al.* Caco-2 permeability of weakly basic drugs predicted with the double-sink PAMPA method. *Eur. J. Pharm. Sci.* **24**, 333–349 (2005).
- 37. Williams, F. M. EDETOX. Evaluations and predictions of dermal absorption of toxic chemicals. *Int. Arch. Occup. Environ. Health* 77, 150–151 (2004).
- 38. Lomize, M. A. *et al.* PerMM: A Web Tool and Database for Analysis of Passive Membrane Permeability and Translocation Pathways of Bioactive Molecules. *J Chem Inf Model* **59**, 3094–3099 (2019).
- 39. RDKit: Open-source cheminformatics. Available 11/6/2023 at https://www.rdkit.org.
- 40. Kim, S. et al. PubChem 2023 update. Nucleic Acids Res. 51, D1373–D1380 (2023).
- 41. Wishart, D. S. DrugBank: a comprehensive resource for in silico drug discovery and exploration. *Nucleic Acids Res.* **34**, D668–D672 (2006).
- 42. Hastings, J. *et al.* ChEBI in 2016: Improved services and an expanding collection of metabolites. *Nucleic Acids Res.* 44, D1214–D1219 (2016).
- 43. Davies, M. *et al.* ChEMBL web services: streamlining access to drug discovery data and utilities. *Nucleic Acids Res.* **43**, W612–W620 (2015).
- 44. Berman, H. M. et al. The Protein Data Bank. Nucleic Acids Res. 28, 235–42 (2000).
- 45. Juračka, J., Šrejber, M., Melíková, M., Bazgier, V. & Berka, K. MolMeDB: Molecules on Membranes Database. *Database* **2019**, (2019).
- 46. Abdalla, M. & McGaw, L. Natural Cyclic Peptides as an Attractive Modality for Therapeutics: A Mini Review. *Molecules* **23**, 1–19 (2018).
- 47. Ho, S. *et al.* The Mechanism of Action of Cyclosporin A and FK506. *Clin. Immunol. Immunopathol.* **80**, S40–S45 (1996).
- 48. Loosli, H.-R. *et al.* Peptide conformations. Part 31. The conformation of cyclosporin a in the crystal and in solution. *Helv. Chim. Acta* **68**, 682–704 (1985).

- 49. Kessler, H., Köck, M., Wein, T. & Gehrke, M. Reinvestigation of the Conformation of Cyclosporin A in Chloroform. *Helv. Chim. Acta* **73**, 1818–1832 (1990).
- 50. Jin, L. & Harrison, S. C. Crystal structure of human calcineurin complexed with cyclosporin A and human cyclophilin. *Proc. Natl. Acad. Sci.* **99**, 13522–13526 (2002).
- 51. Wang, C. K., Swedberg, J. E., Harvey, P. J., Kaas, Q. & Craik, D. J. Conformational Flexibility Is a Determinant of Permeability for Cyclosporin. *J. Phys. Chem. B* **122**, 2261–2276 (2018).
- 52. Wiedmann, T. S., Trouard, T., Shekar, S. C., Polikandritou, M. & Rahman, Y.-E. Interaction of cyclosporin A with dipalmitoylphosphatidylcholine. *Biochim. Biophys. Acta Biomembr.* **1023**, 12–18 (1990).
- 53. O'Leary, T. J., Ross, P. D., Lieber, M. R. & Levin, I. W. Effects of cyclosporine A on biomembranes. Vibrational spectroscopic, calorimetric and hemolysis studies. *Biophys. J.* **49**, 795–801 (1986).
- 54. Söderlund, T., Lehtonen, J. Y. A. & Kinnunen, P. K. J. Interactions of Cyclosporin A with Phospholipid Membranes: Effect of Cholesterol. *Mol. Pharmacol.* **55**, 32–38 (1999).
- 55. Ito, K., Passioura, T. & Suga, H. Technologies for the Synthesis of mRNA-Encoding Libraries and Discovery of Bioactive Natural Product-Inspired Non-Traditional Macrocyclic Peptides. *Molecules* 18, 3502–3528 (2013).
- 56. Omura, T. Mitochondrial P450s. Chem. Biol. Interact. 163, 86–93 (2006).
- 57. Chien, Y., Rosal, K. & Chung, B. Function of CYP11A1 in the mitochondria. *Mol. Cell. Endocrinol.* **441**, 55–61 (2017).
- 58. Schwarz, D. *et al.* Direct visualization of a cardiolipin-dependent cytochrome P450scc-induced vesicle aggregation. *J. Struct. Biol.* **113**, 207–215 (1994).
- 59. Waterman, M. R. & Simpson, E. R. Regulation of the biosynthesis of cytochromes P-450 involved in steroid hormone synthesis. *Mol. Cell. Endocrinol.* **39**, 81–89 (1985).
- 60. Miller, W. L. Steroid hormone synthesis in mitochondria. *Mol. Cell. Endocrinol.* **379**, 62–73 (2013).
- 61. Spinello, A., Ritacco, I. & Magistrato, A. The Catalytic Mechanism of Steroidogenic Cytochromes P450 from All-Atom Simulations: Entwinement with Membrane Environment, Redox Partners, and Post-Transcriptional Regulation. *Catalysts* 9, 1–22 (2019).
- 62. Berka, K., Paloncýová, M., Anzenbacher, P. & Otyepka, M. Behavior of human cytochromes P450 on lipid membranes. *J. Phys. Chem. B* **117**, 11556–11564 (2013).
- 63. Edwards, R. J., Murray, B. P., Boobis, A. R. & Davies, D. S. Identification and location of alpha-helices in mammalian cytochromes P450. *Biochemistry* **28**, 3762–3770 (1989).
- 64. Pikuleva, I. A. Putative F–G loop is involved in association with the membrane in P450scc (P450 11A1). *Mol. Cell. Endocrinol.* **215**, 161–164 (2004).
- 65. Headlam, M. J., Wilce, M. C. J. & Tuckey, R. C. The F–G loop region of cytochrome P450scc (CYP11A1) interacts with the phospholipid membrane. *Biochim. Biophys. Acta Biomembr.* **1617**, 96–108 (2003).
- 66. Ingelman-Sundberg, M., Haaparanta, T. & Rydstroem, J. Membrane charge as effector of cytochrome P-450LM2 catalyzed reactions in reconstituted liposomes. *Biochemistry* **20**, 4100–4106 (1981).
- 67. Ahn, T., Guengerich, F. P. & Yun, C.-H. Membrane insertion of cytochrome P450 1A2 promoted by anionic phospholipids. *Biochemistry* **37**, 12860–12866 (1998).
- 68. Ingelman-Sundberg, M., Hagbjörk, A.-L., Ueng, Y.-F., Yamazaki, H. & Guengerich, F. P. High rates of substrate hydroxylation by human cytochrome P450 3A4 in reconstituted membranous vesicles: Influence of membrane charge. *Biochem. Biophys. Res. Commun.* 221, 318–322 (1996).
- 69. Fleischer, S., Rouser, G., Fleischer, B., Casu, A. & Kritchevsky, G. Lipid composition of mitochondria from bovine heart, liver, and kidney. *J. Lipid Res.* **8**, 170–180 (1967).
- 70. Schwarz, D., Kruger, V., Chernogolov, A. A., Usanov, S. A. & Stier, A. Rotation of Cytochrome P450SCC (CYP11A1) in Proteoliposomes Studied by Delayed Fluorescence Depolarization. *Biochem. Biophys. Res. Commun.* **195**, 889–896 (1993).
- 71. Kisselev, P. et al. Branched Phosphatidylcholines Stimulate Activity of Cytochrome

- P450SCC (CYP11A1) in Phospholipid Vesicles by Enhancing Cholesterol Binding, Membrane Incorporation, and Protein Exchange. *J. Biol. Chem.* **273**, 1380–1386 (1998).
- 72. Navrátilová, V., Paloncýová, M., Kajšová, M., Berka, K. & Otyepka, M. Effect of cholesterol on the structure of membrane-attached cytochrome P450 3A4. *J. Chem. Inf. Model.* **55**, 628–635 (2015).
- 73. Navrátilová, V., Paloncýová, M., Berka, K. & Otyepka, M. Effect of lipid charge on membrane immersion of cytochrome P450 3A4. *J. Phys. Chem. B* **120**, 11205–11213 (2016).
- 74. Baylon, J. L., Lenov, I. L., Sligar, S. G. & Tajkhorshid, E. Characterizing the membrane-bound state of cytochrome P450 3A4: Structure, depth of insertion, and orientation. *J. Am. Chem. Soc.* **135**, 8542–8551 (2013).
- 75. Murtazina, D. *et al.* Membrane-Protein Interactions Contribute to Efficient 27-Hydroxylation of Cholesterol by Mitochondrial Cytochrome P450 27A1. *J. Biol. Chem.* 277, 37582–37589 (2002).
- 76. Cojocaru, V., Winn, P. J. & Wade, R. C. The ins and outs of cytochrome P450s. *Biochim. Biophys. Acta Gen. Subj.* **1770**, 390–401 (2007).
- 77. Bayburt, T. H., Carlson, J. W. & Sligar, S. G. Single molecule height measurements on a membrane protein in nanometer-scale phospholipid bilayer disks. *Langmuir* **16**, 5993–5997 (2000).
- 78. Liu, J., Tawa, G. J. & Wallqvist, A. Identifying cytochrome P450 functional networks and their allosteric regulatory elements. *PLoS One* **8**, e81980 (2013).
- 79. Bridges, A. *et al.* Identification of the binding site on cytochrome P450 2B4 for cytochrome b 5 and cytochrome P450 reductase. *J. Biol. Chem.* **273**, 17036–17049 (1998).
- 80. Estrada, D. F., Laurence, J. S. & Scott, E. E. Cytochrome P450 17A1 interactions with the FMN domain of its reductase as characterized by NMR. *J. Biol. Chem.* **291**, 3990–4003 (2016).